JGR Space Physics

RESEARCH ARTICLE
10.1029/2020JA028884

Short-Term Variability of Equatorial Electrojet Modulation by Solar Tidal and Planetary Waves, as Derived From the Swarm Constellation

Hermann Lühr[1], Yun-Liang Zhou[2], and Patrick Alken[3,4]

[1]GFZ, German Research Centre for Geosciences, Section 2.3, Geomagnetism, Potsdam, Germany, [2]Department of Space Physics, School of Electronic Information, Wuhan University, Wuhan, China, [3]Cooperative Institute for Research in Environmental Sciences, University of Colorado Boulder, Boulder, CO, USA, [4]National Centers for Environmental Information, NOAA, Boulder, CO, USA

Key Points:

- First study of short-term variability of tidal and planetary wave influences on equatorial electrojet (EEJ) based on dual-point observations of the Swarm mission
- The tidal EEJ week-to-week variability is related to intra-seasonal source fluctuations and local time dependent amplitude variations
- First time investigation of EEJ modulation by ultra-fast Kelvin waves and their short-term characteristics

Supporting Information:

Supporting Information may be found in the online version of this article.

Correspondence to:

Y.-L. Zhou,
zhouyl@whu.edu.cn

Citation:

Lühr, H., Zhou, Y.-L., & Alken, P. (2021). Short-term variability of equatorial electrojet modulation by solar tidal and planetary waves, as derived from the Swarm constellation. *Journal of Geophysical Research: Space Physics*, *126*, e2020JA028884. https://doi.org/10.1029/2020JA028884

Received 28 OCT 2020
Accepted 14 APR 2021

Abstract ESA's constellation mission Swarm with its three identical spacecraft allows the separation of spatial and temporal variations of wave phenomena. Here we investigate the modulation of the equatorial electrojet (EEJ) amplitude by solar tides and planetary waves. This is the first study to exploit the short-term variability of these signals in the EEJ. Based on 6-day data sets of quasi-simultaneous observations from the well separated Swarm A and Swarm B spacecraft we derive amplitudes and phases of solar tides and prominent planetary waves. Tidal amplitudes can vary by a factor of 2 from week to week. Conversely, the phases of the tides show steady changes, suggesting a stable tidal system. Simultaneous observations at different local times return quite different wave forms, suggesting local time dependent amplitude changes of the tidal signatures in EEJ. DE3 signatures get weak toward evening, while DE2 is strongest around 15:00 magnetic local time. Modulation of the EEJ by planetary waves up to 6 days is also analyzed. Clearly dominating is the westward propagating quasi-6-day wave. Derived amplitudes are largest around September and exhibit a secondary occurrence maximum at spring time. Generally, the influence of this planetary wave on the EEJ hardly reaches 30% of that caused by solar tides. For the first time we monitor the influence of eastward propagating ultra-fast Kelvin waves at 2–3 days period on the EEJ. Related activity occurs sporadically at intervals of 1–4 months and the effects on the EEJ are even smaller than that from the 6-day wave.

1. Introduction

The Earth's atmosphere exhibits oscillations at a number of different wave modes. Prominent examples are tides. These forced global-scale oscillations are driven either by gravity or heating. For example, solar tides have periods of a solar day or harmonics of it. Most prominent are the westward propagating migrating tides, which follow the apparent motion of the sun around Earth. The so-called non-migrating tides are excited for instance by zonal asymmetries (i.e., topography, land-sea differences, longitude dependences in absorbing species) (Forbes, Hagan, et al., 2003) or by nonlinear interactions between the migrating diurnal tide and planetary waves (Hagan & Roble, 2001). An important source of non-migrating tides, which is responsible for the observed longitudinal wavenumber-4 structure, is latent heat release in the tropical troposphere (Hagan & Forbes, 2002). The zonal wavenumber, s, of non-migrating tides is either negative for eastward (E) propagating ($s < 0$) or positive for westward (W) propagating ($s > 0$) waves. In the case of $s = 0$ waves are stationary. Opposed to migrating tides s is not equal to their frequency (in cycles per day).

Another type of prominent waves is the planetary waves (PW). They belong to the group of planetary-scale atmospheric free resonant oscillations (normal modes). Typically, PW can be found at periods of about 2, 6, 10, and 16 days. They mostly propagate westward with zonal wavenumber 1 ($s = 1$). Occasionally, also eastward propagating PWs and other wavenumbers are observed. For basic details of planetary waves, the reader is referred to the tutorials by Salby (1984) and Forbes (1995) and references therein.

In a more recent study, Forbes and Zhang (2017) described the climatological properties of quasi-6-day PWs in the stratosphere and mesosphere. Their investigations, based on TIMED/SABER temperature measurements between 20 and 110 km altitude and ±50° latitude during 2002–2015, reveal the characteristic distribution patterns of the 6-day wave. Particularly in the mesosphere they develop largest amplitudes around

40° latitude in both hemispheres. Preferred seasons are spring and late summer/fall. Near the equator the quasi-6-day wave signal is generally weak. Only around August appreciable amplitudes are observed.

In this study we focus on the equatorial electrojet (EEJ). The EEJ is a special phenomenon at the magnetic equator in the E region of the Earth's ionosphere, representing a narrow band of enhanced electric current flowing generally eastward during daytime at an altitude of about 108 km (e.g., Forbes, 1981). Here we are mainly interested in the modulation of its amplitude by atmospheric tides and waves. Recently Yamazaki et al. (2018) presented a study on the quasi-6-day wave modulation of the EEJ. They were searching in one-month long data sets for PW signals in EEJ amplitude variations. Prominent quasi-6-day waves were detected in five cases within the period 2006 to 2016. From the five events four occurred in August/September and one in May. This suggests a preference of PW activity near the equator during late summer/fall, consistent with the quasi-6-day amplitude maximum in the mesosphere at low latitudes, as reported by Forbes and Zhang (2017).

Kelvin waves are another class of atmospheric resonant oscillations. Commonly, they are related to latent heat release in the tropics (e.g., Salby & Garcia, 1987). In the literature one finds descriptions of three distinct types of these wave. The slow Kelvin waves (periods 15–20 days) have short vertical wavelengths (~10 km). The fast Kelvin waves (6–10 days) have longer wavelengths (~20 km) and thus can propagate to larger heights. Finally, the ultra-fast Kelvin waves (UFKW) come at periods of 2–5 days and vertical wavelengths exceeding 40 km (e.g., Forbes, 2000; Salby et al., 1984). Due to their short period and long wavelength UFKW are able to reach the lower thermosphere and ionosphere. By studying temperature variations of the middle and upper atmosphere with the SABER instrument Forbes, Zhang, et al. (2009) confirmed that equatorial Kelvin waves reach greater heights the shorter the periods are. Peak wave amplitudes were found at about 105 km and periods of 2–3 days. These authors also showed that UFKW activity is well confined to equatorial latitudes.

UFKW can make important contributions at low-latitude to vertical coupling from the troposphere to the upper atmosphere. England, Liu, et al. (2012) report on radar observations that reveal a 3-day modulation of diurnal tides up to altitudes of 115–145 km in meridional wind measurements. This result is interpreted as a non-linear interaction between the UFKW and the diurnal tide at mesosphere altitudes. Influences of UFKW on the electrodynamics in the ionosphere were presented by Gu et al. (2014). These authors investigated the modulation of electron density and total electron content (TEC) by UFKW. They found prominent variation in the equatorial ionization anomaly (EIA) at period of 2–5 days. These results are interpreted as modulation of the equatorial electric field at E-layer altitude by UFKW that is controlling the ion fountain effect. To the authors best knowledge there has been so far no study investigating the influence of UFKW on low-latitude currents, such as the EEJ.

In addition, we look also at the prominent modulation of the EEJ by non-migrating tides. In the past numerous investigations have shown evidence that the upper atmosphere and ionosphere is subject to forcing by solar non-migrating tides. For example, Sagawa et al. (2005) were the first to show wavenumber-4 variations in the 135.6 nm airglow emissions, observed by the IMAGE-FUV instrument. Subsequently, Immel et al. (2006) interpreted these longitudinal patterns as the eastward propagating diurnal non-migrating tide, DE3, originated from the lower atmosphere, and driven by deep tropical convection (Hagan & Forbes, 2002). Subsequently, the influence of solar non-migrating tides on the ionosphere and thermosphere was revealed in many studies. For an overview see, for example, the review articles by England (2012). Signatures of non-migrating tides in EEJ amplitude variations have also been a subject of great interest (e.g., Alken & Maus, 2010; England, Maus, et al., 2006; Lühr & Manoj, 2013; Lühr, Rother, Häusler, Alken, & Maus, 2008; Zhou, Lühr, Xu, & Alken, 2018). They reveal the great diversity of solar tidal components influencing the electrojet.

All the aforementioned studies focus on the mean features of solar tides and planetary waves in the EEJ. They look at the averages of observations covering several months or even several years. Those studies helped us to get a good understanding of the climatological features of these waves. However, the short-term variation of solar tides and PWs in the EEJ are not yet clear. Pedatella, Oberheide, et al. (2016) performed some model analysis, making use of the Whole Atmosphere Community Climate Model (WACCM) combined with the Data Assimilation Research Testbed (DART) framework for estimating the variability

of the diurnal tidal component, DE3. Obtained results reveal significant amplitude changes on 10–20 day time-scales. Furthermore, the authors state a lack of direct knowledge about the DE3 short-term variability due to limitations in current observations, which restrict tidal analysis primarily to seasonal variability. To our knowledge, this is the first detailed observation-based study on short-term wave variability of the electrojet on a global scale.

For investigating these variations, simultaneous EEJ observations at longitudinally well-separated locations are required. With the help of the unique Swarm satellite constellation, we are able to provide this missing information. In the present study we make use of EEJ current density estimates derived from the magnetic readings of Swarm A and Swarm B during March 2014 to March 2021. Due to the slight difference in inclination, the orbital planes of Swarm A and Swarm B separate slowly with time. During the considered years the spacecraft scanned through all possible longitudinal differences. For the wave analysis data sets over 6 days are taken into account. This provides the week-to-week variability of the EEJ modulation by tides and planetary waves.

In Section 2 we will describe the Swarm constellation and the data set. Our approach to derive the solar tides and planetary waves will be presented in Section 3. The observational results are shown in Section 4. Then, in Section 5, we will discuss our observational results in the context of previous studies. The main findings are summarized in Section 6.

2. Swarm Constellation and Data Set

ESA's Swarm mission comprises three spacecraft, namely Swarm A, B, and C. They were launched together into a near-polar orbit on November 22, 2013. Their initial orbits were at the altitude of about 490 km with an inclination of 87.5°. From January 2014 onward the Swarm A, B, and C spacecraft were maneuvered apart and achieved the final constellation on 17 April 2014. In this constellation, Swarm A and C fly side-by-side at an altitude of about 450 km and with an inclination of 87.35°. Swarm B cruises at about 510 km, about 60 km higher, and at an orbital inclination of 87.75°. Due to the slightly higher inclination of Swarm B compared to the pair Swarm A/C the orbital plane of Swarm B precesses somewhat slower through local time. As a consequence, an angular difference builds up between the two orbital planes, starting in the middle of February 2014 and amounting to 24° per year. This is equivalent to a growing difference in local time. Swarm B lags behind Swarm A/C and the difference increases by one hour in local time every 232 days. At the start of 2018 both orbits were 90° apart, and both planes are expected to become coplanar again (but counter-rotating) during fall 2021. For more details about the Swarm mission and its instruments the reader is referred to Friis-Christensen et al., (2008).

Figure 1a shows the local time (LT) evolution of the dayside equator crossings. Swarm A (blue curve) needs about 133 days to cover the sector 06–18 LT, and Swarm B (red curve) requires for that sector about 140 days. This provides us the opportunity to sample the EEJ almost simultaneously at two local times.

The orbital periods of Swarm A and B are somewhat different because of the greater height of Swarm B. As a consequence, Swarm A will overtake Swarm B every few days. Since the lower orbit of Swarm A decays faster than that of Swarm B, the time period for overtaking becomes progressively shorter. Figure 1b shows the evolution of time differences between adjacent overtakings. In the beginning (March 2014) it takes more than 6 days, but it decreases in 2021 to about 4 days. These periods between quasi-simultaneous equator crossings are of particular interest in this study. They provide dual-point EEJ samplings well-distributed over all longitudes. This promises to offer more information about the short-term variability of the EEJ modulation by tides and waves.

The basis for our analysis is the height-integrated peak current density of the EEJ, which is derived from the magnetometer measurements onboard Swarm A and B from March 2014 to March 2021. Here we prefer to interpret the derived current density distribution rather than the magnetic field profiles for characterizing the electrojet intensity because the current values are in principle independent of the measurement height. This is important for bringing all the data considered here on the same level. In this way we account for the orbit decays over the years and for the height difference of more than 60 km between Swarm A and B.

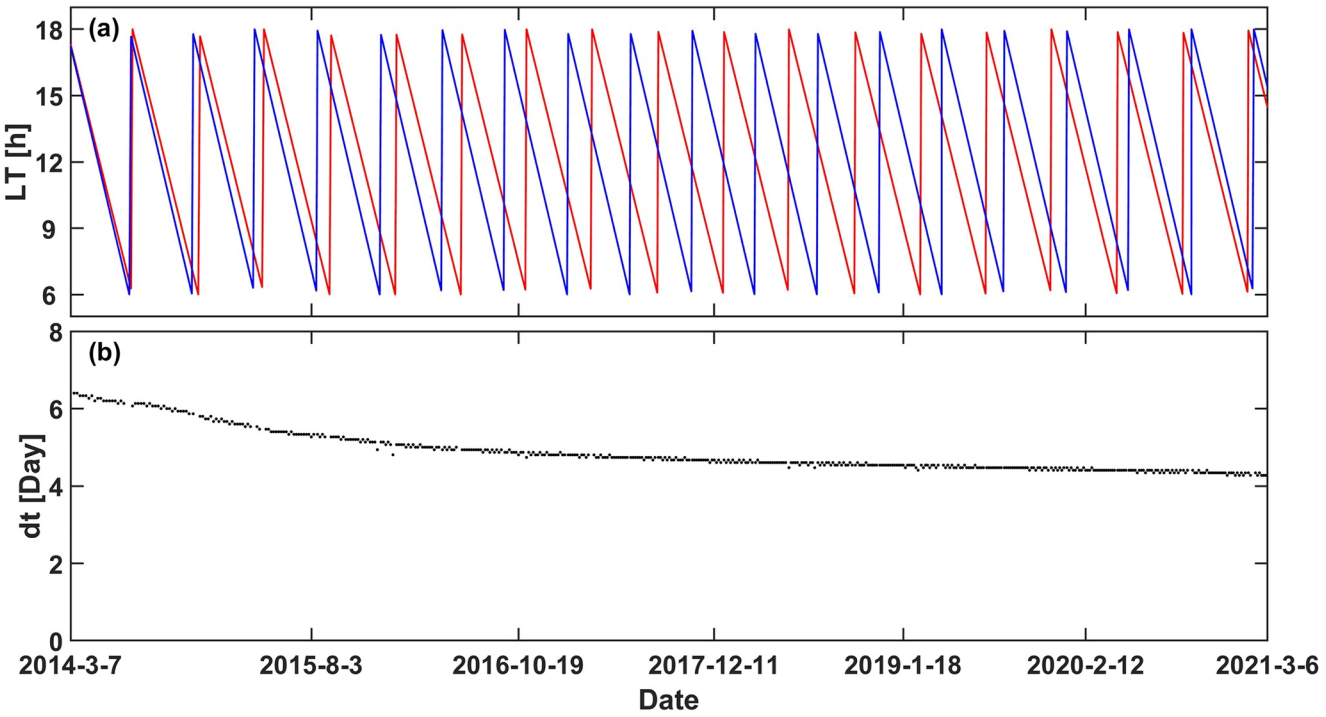

Figure 1. (a) Evolution of Swarm A (blue) and Swarm B (red) local time variation of dayside equator crossings. (b) Evolution of time differences, dt in days, between quasi-simultaneous Swarm A and B equator crossings on the dayside. Due to the faster Swarm A orbit decay the times between orbital overtakings become successively shorter.

The processed Swarm EEJ height-integrated current density data sets are available at the website (https://earth.esa.int/web/guest/swarm/data-access). For deriving the EEJ latitude profiles from the magnetic readings, we first remove the main, crustal, and magnetospheric fields from the magnetic observations. The core field strength is subtracted from the Absolute Scalar Magnetometer (ASM) measurements by using a core field model (Alken, Maus, Chulliat, Vigneron, et al., 2015). By means of the MF7 model (Maus, Yin, Lühr, et al., 2008), we removed the crustal field contributions. With the help of the external field part of POMME-6 (Lühr & Maus, 2010) the magnetospheric fields can also be subtracted from the magnetic measurements. Finally, the contribution from Sq currents at middle latitudes and unmodeled external fields are filtered out on a track-by-track basis. These operations result in clean EEJ magnetic signals. By using a model of line currents flowing along constant quasi-dipole latitudes at 110 km altitude in the equatorial E region, we derive, by inverting the magnetic signals, the EEJ profiles of height-integrated sheet current density. For a more detailed description of calculating the EEJ current density, the readers are referred to Alken, Maus, Chulliat, and Manoj (2015) and Alken (2020).

3. Calculation of Tides and Waves

Earlier studies of the EEJ tidal characteristics have generally focused on the mean values by averaging the data over months or even years. Here we want to investigate the variability on about weekly basis. As a suitable data set for those studies, the period between two quasi-simultaneous Swarm equator crossings has been identified. We have searched for epochs when the time difference between the equator crossings of Swarm A and Swarm B is smallest. This epoch is taken as the beginning of the individual data sets. Since we have data of somewhat less than a week between quasi-simultaneous equator crossings, we can analyze non-migrating tides and planetary wave up to a 6 day period. Due to the faster orbital decay of Swarm A, the period between overtakings becomes progressively shorter, as can be seen in Figure 1b. For that reason, we decided to take just 6 days for each data set, but start all the data sets at the epochs of quasi-simultaneous equator crossings. This provides some overlap of data sets during later years, but it ensures an equal data volume for all the events.

In a first step we estimated the modulation of the EEJ by non-migrating tides. Here we are primarily interested in a good temporal resolution. Therefore, we have to make compromises in the spectral resolution. Due to the fairly small individual data sets and their limitation to one point in local time, all the tidal harmonics of a day with their various azimuthal wavenumbers cannot be resolved. For that reason, we have restricted the analysis to the wavenumber 1–4 spectra in the local time frame. Although lacking tidal resolution, this covers practically the whole solar tidal signal.

For deriving quantitative values of the amplitudes and phases we fit, after removal of any linear trend, the tidal functions separately to the 6-day data sets of Swarm A and Swarm B. The wavenumber spectrum can be expressed in the form

$$\mathrm{EEJ}_{\mathrm{tide}} = \sum_{n=1}^{4} A_n \cos\left(n\lambda - \phi_n\right) + C \tag{1}$$

where A_n are the amplitudes and ϕ_n are the phases of the wavenumber components; n is the wavenumber index (WN-n), λ is the longitude, C denotes the constant term; Based on earlier experience (e.g., Lühr & Manoj, 2013) we have limited the spectrum from WN-1 to WN-4. The additive constant, C, reflects the mean EEJ amplitude during the 6 days. For the analysis only EEJ readings of the local times from 06:30 to 17:30 MLT have been considered. During the dark hours the EEJ practically vanishes. For a 6-day data set the local time is considered to be constant. Thus, the amplitudes and phases of the tides with zonal wavenumbers, obtained from a 6-day data set, are assigned to their mean local time.

It is known that the amplitude of the EEJ varies greatly with local time. This is mainly due to the change of solar zenith angle (SZA) and the associated variation of the ionospheric conductivity. According to Chapman's theory the E-region conductivity should vary as the square root of cos(SZA). In order to compensate for the diurnal conductivity variation, we have normalized all EEJ amplitudes by dividing the observed values by the square root of cos(SZA).

At certain times the electrojet is disturbed, for example during periods of enhanced magnetic activity. Then spurious EEJ peak values may result. For omitting those we make use of a robust function fitting procedure of Equation 1. In our approach we first fit Equation 1 to the 6-day data set of EEJ current density and obtain the initial amplitudes and phases of the non-migrating tides with wavenumbers 1–4. Then we calculate the average value and standard deviation (σ) of the difference between the observation and the obtained initial tidal results. In a second step only the observations that are located within the 2σ limit of the initial tidal curve, are utilized. With those the improved fitting is performed. By this procedure only 5% of data points are excluded, and there are almost twice as many negative values as positive. Enhanced magnetic activity is known to be an important driver for the counter electrojet. From the final results amplitudes and phases of the tides with wavenumber 1–4 are derived. These values form the data basis of the following non-migrating tidal analysis.

Besides the solar tides we are also interested in the planetary and Kelvin wave activity influencing the electrojet. As will be shown in the next section, the non-migrating tides and the planetary waves are functionally well decoupled and can thus be determined independently. For that reason, we estimate first the tidal signals individually from Swarm A and Swarm B data. In a next step we subtract the derived tidal functions from the EEJ data of Swarm A and B. Then the residuals from both spacecraft are combined. This two-spacecraft data set is essential for deriving both the period and propagation direction of the planetary and Kelvin waves that may be active. Furthermore, it assumes that these wave signals do not depend on the local time of sampling.

For deriving the Fourier spectrum of our 6-day data sets we analyze the possible periods. Since the Fourier harmonics are orthogonal functions, we can solve for all the considered periods simultaneously.

$$\mathrm{EEJ}_{\mathrm{PW}} = \sum_{T}\sum_{s}\left[A_{sT}\cos\left(\frac{\Omega t}{T} + s\lambda - \phi_{sT}\right)\right] \tag{2}$$

where T denotes the period, according to the Fourier theorem, in days ($T = 6, 3, 2, 1.5$) and s is the zonal wave number ($s = -1, 1$). Here a positive value of s reflects westward propagation and negative stands for

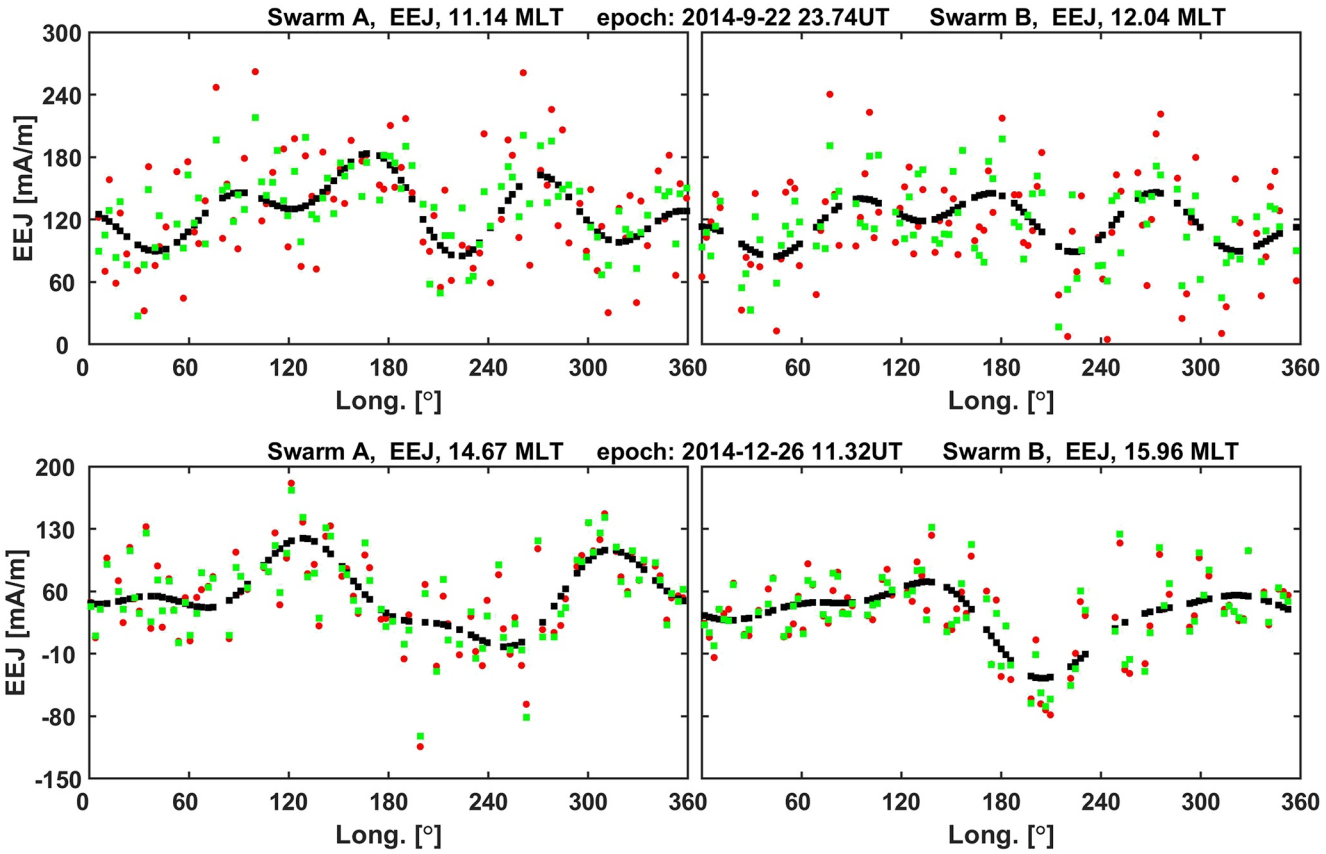

Figure 2. Examples of non-migrating tidal fits to Swarm A (left) and Swarm B (right) longitude variations of equatorial electrojet (EEJ) peak amplitudes. In the top row a case from fall equinox is shown and below from December solstice. The series of black dots represent the derived tidal signal. Red dots are the original EEJ peak amplitudes, and the green dots represent the EEJ readings minus the coestimated planetary waves.

eastward propagation. In this analysis the index $s = 0$ is omitted because stationary planetary waves are included in our tidal analysis, outlined in Equation 1. A_{sT} and ϕ_{sT} are the amplitudes and phases of the related waves with different period and zonal wave number. Ω is the rotation rate of the Earth; t is the UT time and λ is the longitude.

The discrete Fourier spectra analyzed from the 6-day data sets provides only a coarse view of the planetary wave frequency distribution, but it offers well-defined amplitude values. Dynamic spectra with higher period resolution, but relative amplitudes, will be presented in the context of Section 4.4.

4. Observations

In this section we present the spectral results of the EEJ modulation by solar tides and planetary waves. The analysis period is ranging from March 2014 to March 2021. In total about 549 6-day data sets for each spacecraft are taken into account. The average solar activity was fairly low with a mean radio flux index of F10.7 = 91.4 sfu and the mean magnetic activity amounted to Ap = 8.4 nT. The more active time occurred during the first two years.

4.1. Representative Examples

In a first step we have estimated the solar tidal activity of the EEJ. For that purpose, the function representing the first four wavenumber components, as outlined in Equation 1, was fitted to the 6-day data sets, separately for Swarm A and B. Examples for results of such fitting exercises are presented in Figure 2. The top two frames show a case from fall equinox 2014. The series of black dots represents the retrieved tidal

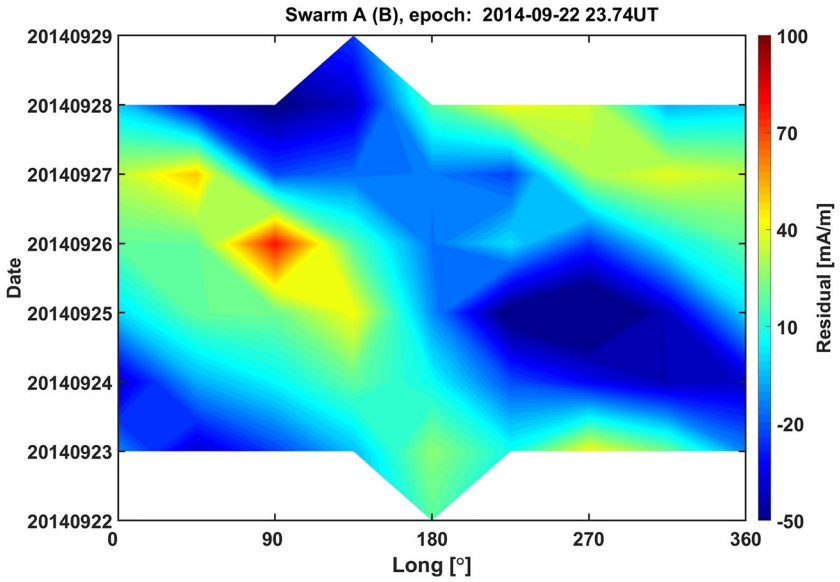

Figure 3. Example of residuals after subtracting the tidal signal from the EEJ peak amplitudes. A clear indication of a 6-day westward propagating wave is observed.

variation over all longitudes. As expected for this season, the wave-4 pattern dominates the longitude variation both at Swarm A (left) and Swarm B (right). In a large number of publications (e.g., England, 2012; Lühr & Manoj, 2013; Oberheide et al., 2006) it has been shown that the diurnal tide DE3, main contributor to the WN-4 signal, peaks around August and September although other tidal components like DW5 and stationary planetary wave, SPW4 also may add to it. The resulting tidal signal at the two spacecraft is similar but not identical. We relate that to the difference in local time by about one hour between the samplings.

The actual EEJ amplitudes (red dots) exhibit a significant scatter about the tidal curve. We attribute that, at least partly, to the activity of planetary waves. Further down in this section characteristics of those waves are addressed. When subtracting the PW signal from the EEJ readings the green dots result, which follow much better the black tidal curve. The remaining scatter of the green dots about the black curve we attribute to external influences on the EEJ, as described for example by Manoj et al. (2008). The EEJ current estimates presented here are highly reliable, as has been demonstrated by Zhou, Lühr, Alken, and Xiong (2016) when comparing results from the close-by orbiting Swarm A and C spacecraft (separated by 1.4° in longitude). Further details about the uncertainty of wave estimates are presented in Section 4.2.

The lower part of Figure 2 shows an example from December solstice 2014. As expected for that season, the tidal signature (black dots) hardly contains any wave-4 pattern. Rather, wave-2 signals are dominating the curve from Swarm A. Conversely, Swarm B returns a mixture of wavenumber 1, 2, and 3 contributions. In this case the differences between the tidal curves of Swarm A and B are quite apparent, but the local time difference between the two spacecraft has meanwhile increased to about 1.5 h. Here the EEJ readings (red dots) follow more closely the tidal curves than in the example above. This suggests a smaller PW activity.

As described in the previous section, we subtracted the derived tidal signal from the EEJ readings individually for both spacecraft. Then the residuals of Swarm A and B are combined for deriving the planetary wave activity. This is justified because the PWs should not depend on local time but just on longitude and UT. The dual-point observations will help to delineate the PW signal from other variations. For supporting these inferences Figure 3 shows the combined EEJ residuals for the event of epoch September 22, 2014 as described above. Clearly visible is the dominating quasi-6-day westward propagating planetary wave. From this plot a PW amplitude of about 40 mA/m can be estimated.

Figure 4 presents the derived planetary wave signals for the two above introduced epochs, fall equinox and December solstice 2014 (same as in Figure 2). Shown is the wave amplitude variation over time for an equatorial station at the 0° longitude. For the September 22, 2014 case we retrieve a dominating 6-day wave that

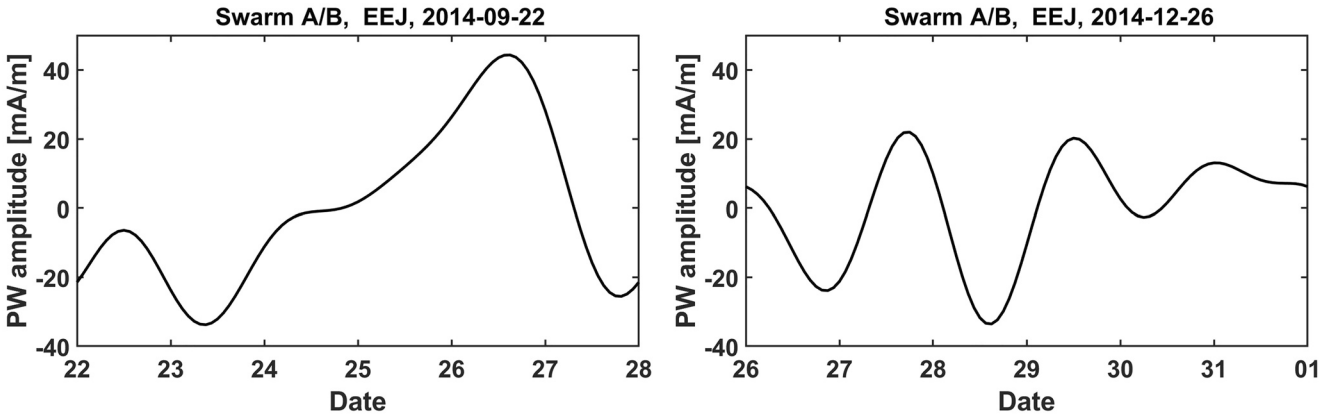

Figure 4. Two examples of planetary wave signature in EEJ amplitude. Shown is the wave signal variation at 0° longitude over the considered 6-day period, as derived from the combined Swarm A and Swarm B residual data sets.

peaks on September 26, with an amplitude of about 40 mA/m. In addition, there is also some 2-day wave present that causes a kind of triangular wave shape. We obtain quite different results for the December 2014 case. Here the wave activity is somewhat smaller and a quasi-2-day wave is dominating.

For checking the reliability of our tidal and wave fitting exercise we have a look at the final residual plots. Figure 5a shows the case for the epoch September 22, 2014. Remaining features are relatively small. Some systematic longitudinal patterns represent a weak westward propagating 6-day wave with wavenumber 2. This may reflect some spectral leakage when imposing our fixed 6-day window onto the quasi-6-day wave. Or it indicates child waves caused by an interaction of this extra ordinary strong quasi-6-day wave with a stationary planetary wave. During other epochs the 6-day wave is weaker and the residuals show a more random distribution, such as Figure 5b.

4.2. Variability of Non-Migrating Tides

After having seen individual cases of EEJ modulation by solar tides we applied the analysis systematically to all the 6-day periods of the Swarm mission. Due to the vanishing amplitude of the EEJ in the morning and evening, we restricted the tidal analysis to the local time period from 6:30 to 17:30 MLT. This causes some gaps in the available data series. For mitigating the effect of diurnal amplitude variation, the EEJ values had

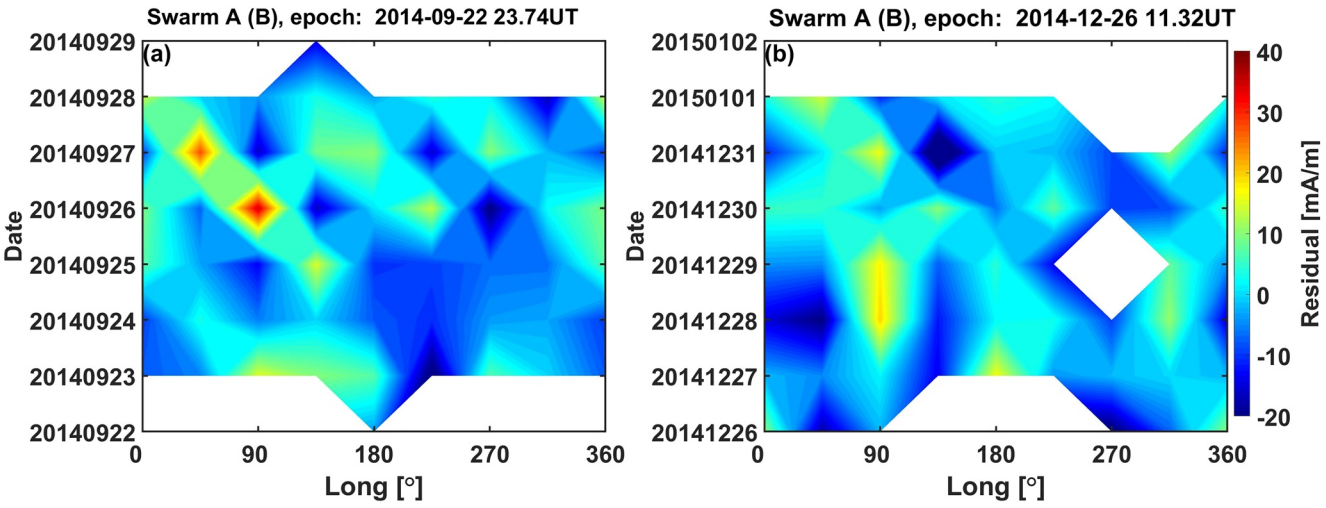

Figure 5. Examples of final residuals after subtracting the tidal signal and the planetary waves from the EEJ amplitudes. Remaining signals reflect higher wavenumber planetary waves and scattered externally driven EEJ variability.

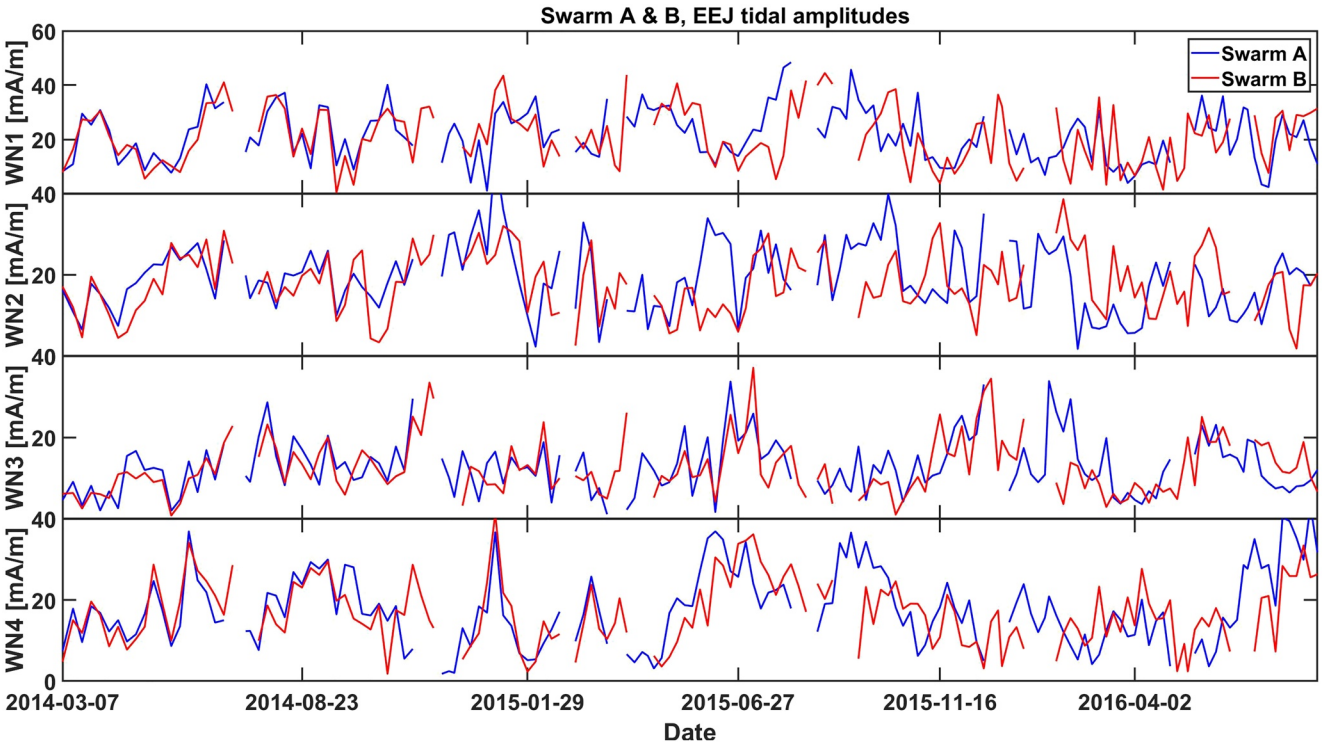

Figure 6. Solar tidal EEJ variability at the wavenumber 1 through 4 components during the 2 years March 2014–August 2016, separately derived from Swarm A and Swarm B.

been normalized to noontime values by considering the solar zenith angle at the observation side, that is, dividing the EEJ amplitudes by the square root of cos(SZA), see Section 3.

Figure 6 shows the temporal variations of the WN-1 through WN-4 amplitudes, separately derived from Swarm A and Swarm B for the first 2 years from March 2014 to August 2016. Related plots for the remaining 5 years can be found in the supporting information to this paper (Text, Figure S1). On the left side, the beginning of the analysis period, the results from the two spacecraft are practically identical. This is expected since the orbital planes are close together. From about 2015 onward, when the local time difference between the spacecraft well exceeds one hour, differences in amplitude can partly be observed between the two sets of tidal components (red and blue curves). However, in general both time series follow similar trends.

For completeness, we derived also the phases for the four wavenumber components. Their interpretation is not so straight forward. Therefore, the results are presented only in the supporting information (Text, Figure S2). Plotted are the longitude values, at which wavenumber signals peak. For the wavenumber 1 component there exists only one peak around the globe, thus the phase can vary between ±180° Lon. In the case of higher harmonics of a day multiple peaks appear. We have selected the one closest to the Greenwich meridian for defining the phase. Therefore, the displayed longitude ranges are reduced in those cases. In the case of a stationary planetary wave the phase is independent of local time, but when non-migrating tides are dominating the longitudinal pattern, the phase should change as the orbit precesses through local times. In the latter case separate phase value curves should appear for Swarm A and Swarm B since they cruise at different local times. Both types of phase curves can be observed.

Generally, we can state, the phase shows relatively small variations on a week-to-week base, quite different from the changes of the amplitude. This suggests a fairly stable driving mechanism.

On average the derived wavenumber components show the expected seasonal variations. For demonstrating that Figure 7 presents the mean seasonal variations over the course of a year separately for the four considered wavenumbers. Most prominent is the well-known peak of WN-4 during late summer to fall. Conversely, WN-3 exhibits maxima, although less prominent, during solstice seasons. Very similar seasonal

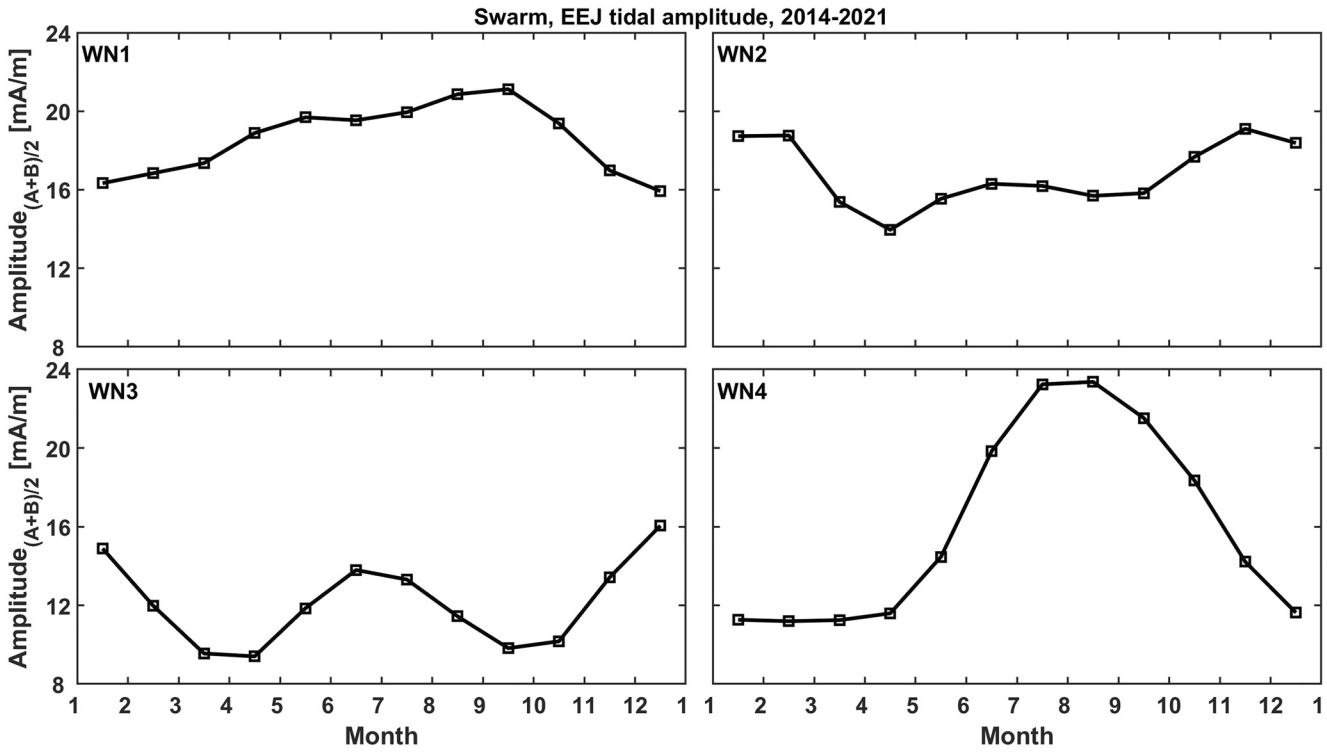

Figure 7. Mean seasonal variation of the EEJ tidal signals, separately for the wavenumber 1 through 4 components. The well-known climatological curves for the different wavenumbers emerge.

variations as our curves in Figure 7 for WN-3 and WN-4 were obtained by Pedatella, Forbes, and Oberheide (2008) (their Figure 1) and Lühr, Rother, Häusler, Fejer, & Alken (2012) (their Figure 4) for the DE2 and DE3 tides, respectively, from CHAMP data analyses. This infers that these two wavenumber structures are primarily driven by the diurnal DE2 and DE3 atmospheric tides. The WN-1 signal peaks around fall season and has its minimum at the beginning of the year. WN-2 attains largest amplitudes around December solstice. This is consistent with the dominant role of SW4 during that season, as reported by Pedatella, Forbes, and Oberheide (2008) and Lühr and Manoj (2013). When adding up the contributions from all components (plot not shown) largest tidal activity results for August and smallest for March, exactly as reported earlier from CHAMP observations (e.g., Lühr & Manoj, 2013). The reproduction of all these well-known average tidal amplitude features adds confidence in the validity of the detailed tidal results derived from our 6-day data sets.

An interesting fact, evident from Figure 6, is the significant variability of the wavenumber amplitudes from week-to-week. This cannot be attributed to the uncertainty of our wave analysis. For estimating the reliability of the presented wave data three aspects have to be considered. The precision of EEJ current estimates is high, as has already been addressed in Section 4.1 by referring to the excellent agreement of EEJ results derived from the closely spaced Swarm A and C satellites. Second, there may be a bias between Swarm A and B EEJ current estimates because of their differences in orbital height. For checking that, we had a look at the first three months of our analysis, when the two orbital planes were close together and the two spacecraft are expected to return the same amplitudes for the wavenumber 1–4 signals from their individual data sets. Figure 8 shows scatter plots of the amplitudes derived by Swarm A versus those from Swarm B. All the points are grouped around the one-to-one dashed lines. It is hard to identify any difference in slope. This confirms that the height of the satellites has no systematic influence on our EEJ current estimates.

Finally, the most important contribution to the uncertainty of our wave analysis comes from the scatter of EEJ intensity due to external influences. For checking that we repeated the analysis of the WN1–4 tidal components twice, using only every second data point (either the even or uneven count numbers from the 6-day data sets). Subsequently, the distribution function of differences between the pairs of amplitudes

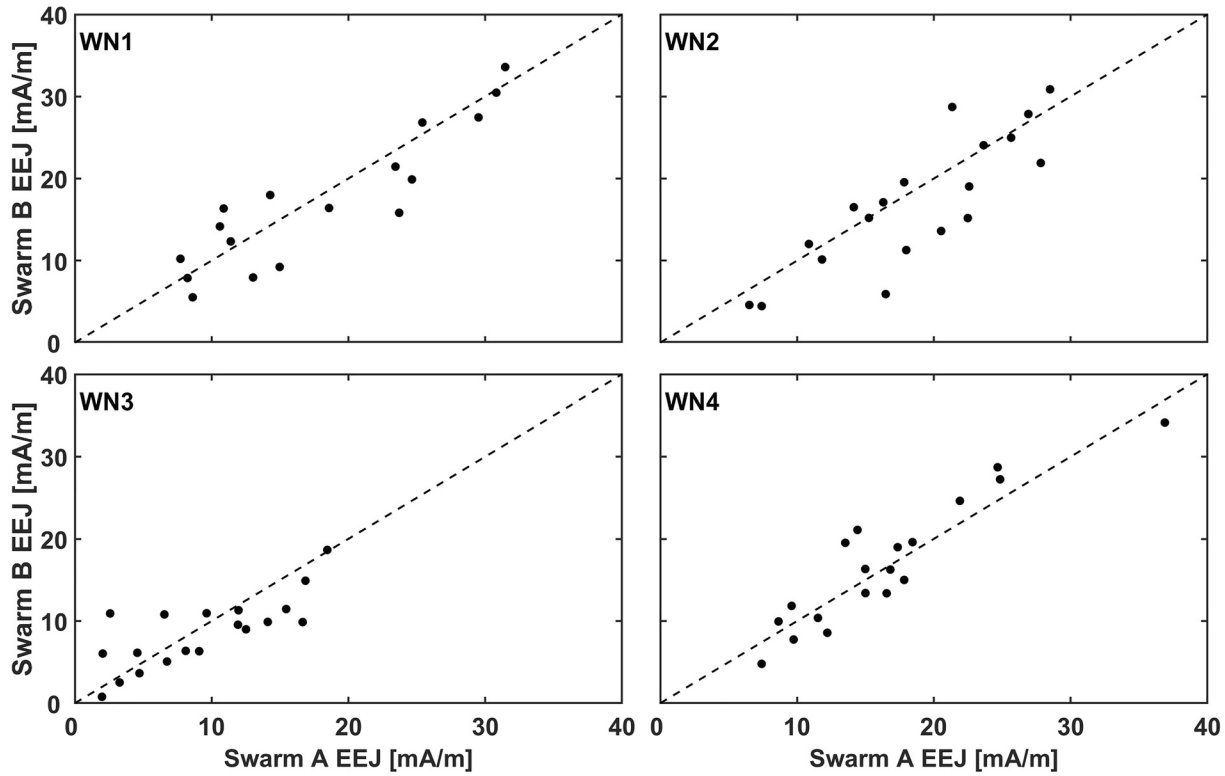

Figure 8. Direct comparison of EEJ tidal signatures derived independently by Swarm A and Swarm B during 3 months of orbiting in near-by planes. No systematic differences can be observed.

from all epochs is plotted and fitted to a Gauss distribution. Figure 9 shows the distribution of differences separately for the wavenumbers 1–4. Here we combined the results from Swarm A and B for getting a better statistic. From the fitted Gauss curves we derive the width of the distribution. For all four wavenumbers good normal distributions result. Since only half the number of data points contributed to the solutions, and since we considered the full differences between individual solutions, the obtained widths are divided by two for getting realistic estimates of our wave analysis uncertainties. Thus, resulting standard deviations are WN-1: 2.9 mA/m, WN-2: 3.3 mA/m, WN-3: 3.2 mA/m, and WN-4: 3.7 mA/m. These numbers are clearly smaller than the derived amplitude variations on weekly time scales.

For explaining the short-term variability there must be processes in the atmosphere-ionosphere system that can change the efficiency of tidal influences on the EEJ on weekly or even shorter time scales. For further investigating the characteristics of the short-term variations we remove the mean seasonal variation of tidal signals by a kind of high-pass filtering. In practice, a low-order (quadratic) polynomial is fitted to the amplitude values over a period of about 140 days. The 140 days just cover all local times. Then the smooth function is subtracted from the individual tidal readings of Figure 6. In the next step the 140-day interval is advanced by one month and the procedure repeated. Figure 10 shows time series of the fluctuations of EEJ tidal signature for all four wave numbers. Horizontal dashed lines mark the levels of standard deviation, as derived above. Amplitudes of the fluctuations in most cases exceed the uncertainty level. Larger variability is observed during the first year, when the solar activity is highest, and it gradually decreases during the following years.

In a quest for processes that may cause the short-term amplitude variability of tidal signatures we tried to identify certain periodicities in the time series. By fitting harmonic functions with periods of 12, 16, 20, 24, ... 180 days to the fluctuations shown in Figure 10 we obtain periodograms for all four wave numbers. Mean spectra are presented in Figure 11. There appear several major peaks. Most of them are in fair agreement between the results from Swarm A and Swarm B. All these peaks can be associated to basic periodicities. The longest, 132 and 140 days are needed by Swarm A and B to cycle through all local times, respectively. This is quite promi-

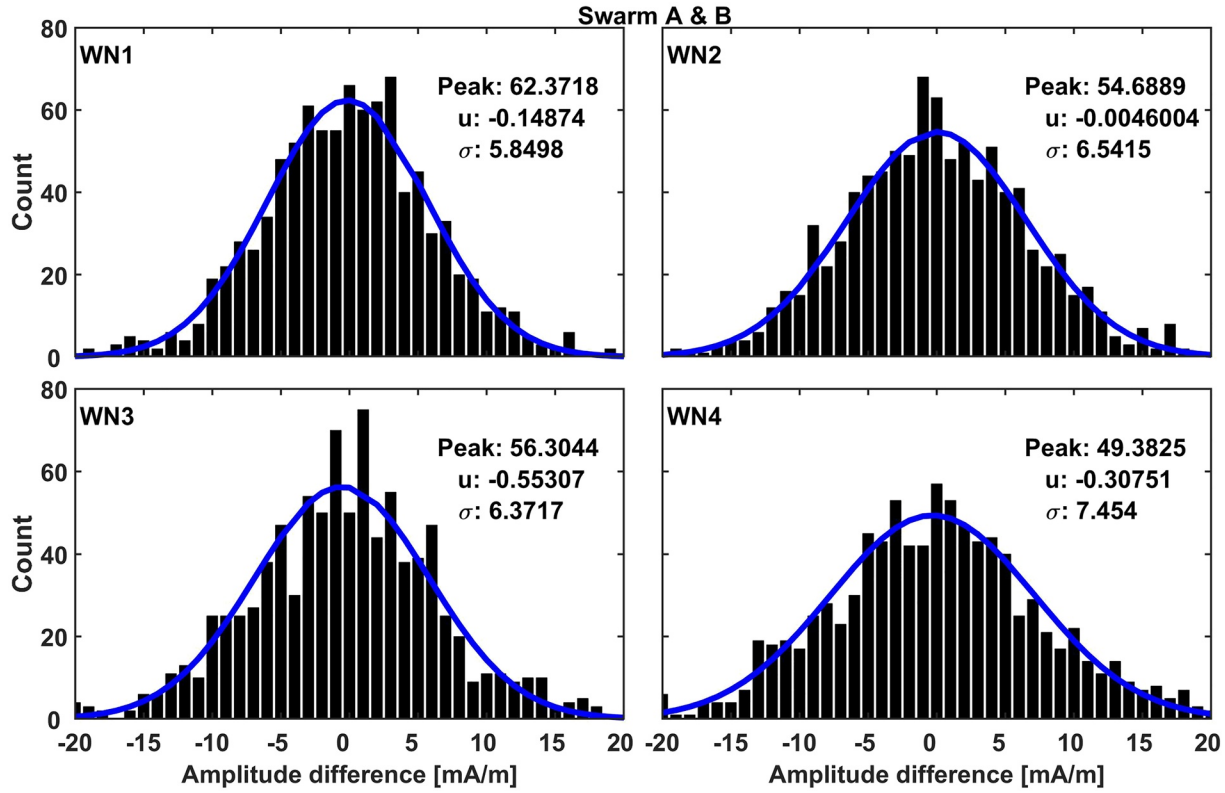

Figure 9. Distribution functions of differences obtained by comparison of two independent tidal signature analyses using only half the data point of the 6-day intervals (either even or uneven counts). The distribution of differences represent for all wavenumber components reasonably well normal Gauss curve (blue curves).

nent in WN-1 and also visible in WN-4. A peak appearing at all wave numbers is 96/100 days for Swarm A/B. This is caused by the modulation of the local time dependence by the annual variation, as can be verified by equation $1/100 = 1/140 + 1/365$. The 76-day period, more prominent in the Swarm A results, reflects the beating of the local time cycle with the semi-annual variation. In some spectra (e.g., WN-2) the 56-day period represents the beating of the half local time cycle with the annual variation. Finally, 32/36 days reflect one quarter of the local time cycle. From these assignments of spectral peaks, we can deduce that the combination of local time dependence and seasonal variation play the main role in causing the short-term variability of the EEJ tidal signatures.

4.3. Local Time Dependence of Tidal Signatures

Results of the spectral analysis show that the amplitudes of tidal effects are quite dependent on local time, and this dependence changes with season. The Swarm satellites provide the opportunity to monitor the tidal signatures of the EEJ quasi-simultaneously at two different local times. From basic tidal analysis it is known that atmospheric tides represent global scale oscillations. If just a single tidal component contributes to a wavenumber its amplitude should be the same at all local times. As a consequence, we may expect longitudinal patterns that shift in longitude with time. However, our dual-satellite observations show that for short-term EEJ tidal signatures this is not true. Already from the example in Figure 2, lower panel, we can reveal a significant difference in tidal signature derived by the two Swarm spacecraft, which are separated by about 1.5 h in local time. From Figure 8 we know that the tidal results of Swarm A and B are practically identical during the first 3 months when the spacecraft orbit close together. But during later months and years partly large differences appear in Figure 6 at all four wavenumbers between the amplitudes derived by Swarm A and Swarm B from data of the same epoch (see also supporting information Text, Figure S1).

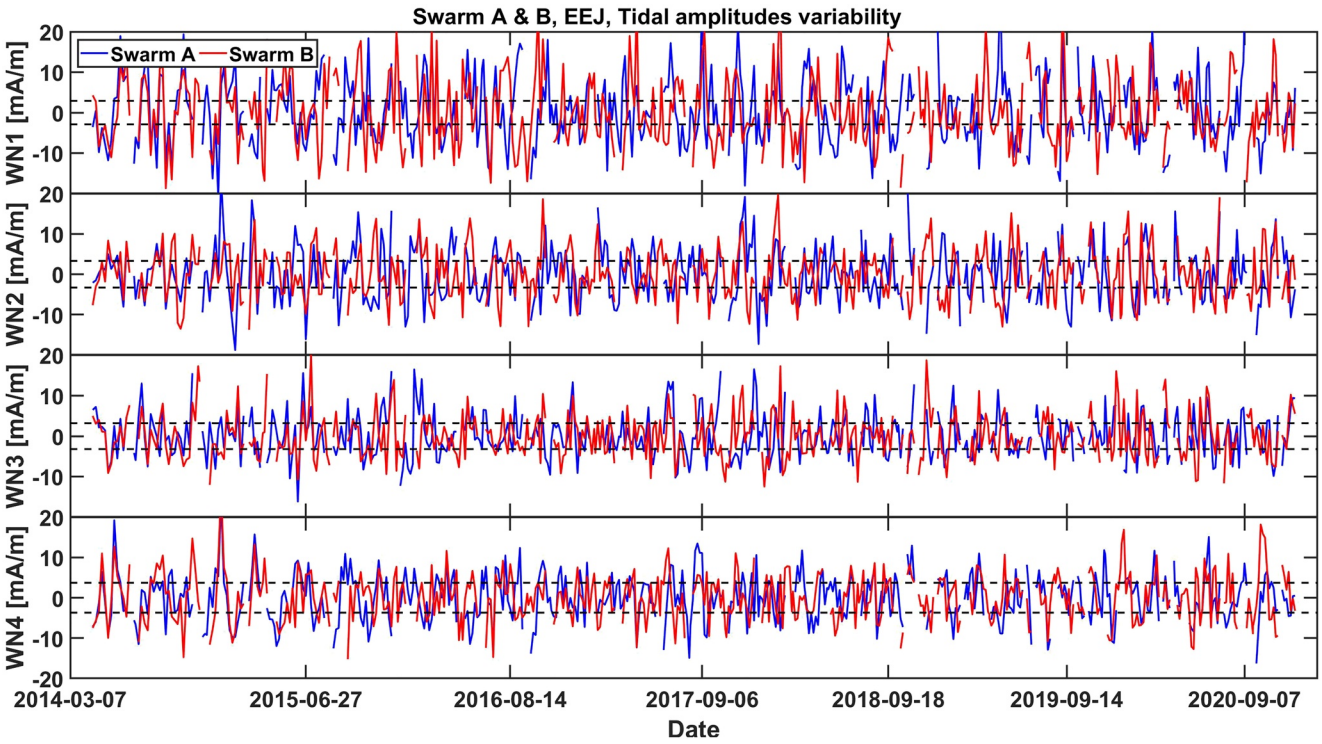

Figure 10. Short-term fluctuation of EEJ tidal signatures. Shown are the high-passed signals from Figure 6. The horizontal dashed lines mark the uncertainty range (±1 standard deviation) of the displayed values.

Two more instructive examples are shown in Figure 12. During the event of November 13, 2017 Swarm A observed a signal containing WN-1 and WN-2 variations, while in the case of Swarm B WN-4 is dominating. This is surprising because, based on seasonal averages, WN-4 is expected to vanish around December solstice. But this is obviously not true for short-term events. In Figure 6 it can be seen that prominent WN-4 amplitudes occasionally are observed during this season. Examples are found in January 2015 and January 2016. Possible explanations for the appearance of WN-4 patterns during months around December will be offered in Section 5.1.

In the event of epoch December 11, 2017 (Figure 12, bottom frames) Swarm A observed mainly a WN-2 tidal signal while in the case of Swarm B WN-3 is dominating. These two tidal components are quite common for the December season. In both examples Swarm B was sampling the EEJ in the morning and Swarm A about 6 h later in the afternoon. The resulting question is: Do the different wavenumber components have preferred local time sectors for modulating the EEJ intensity?

For answering this question, we may look for systematic local time preferences of the four wavenumber signatures. Figure 13 presents an attempt to visualize mean differences of the amplitudes derived simultaneously by Swam A and Swarm B, ordered by local time. Displayed are the mean logarithmic (*ln*) values (arithmetic means) of the amplitude ratios, Swarm A over Swarm B. Values have been sorted into 2 h by 2 h of local time bins. For guiding the eye, diagonal lines are added to the frames. The ascending diagonal marks results of observations where Swarm A and B sampled the EEJ at the same local times. Here we expect comparable values from both spacecraft. That means, the *ln* of the ratio should be close to zero. In principle, this is what we find. Note, for clarity a brown contour line has been added for marking the location of the zero boundary. Furthermore, we can expect that $ln[A(MLT1)/B(MLT2)] = -ln[A(MLT2)/B(MLT1)]$. Therefore, mirror images should appear in the triangles above and below the ascending diagonal. Also that is quite apparent in Figure 13.

Displayed here is the mean situation of the 5 months June to October. During that period tidal signatures attain in general largest amplitudes. The local time dependence during the months December to April,

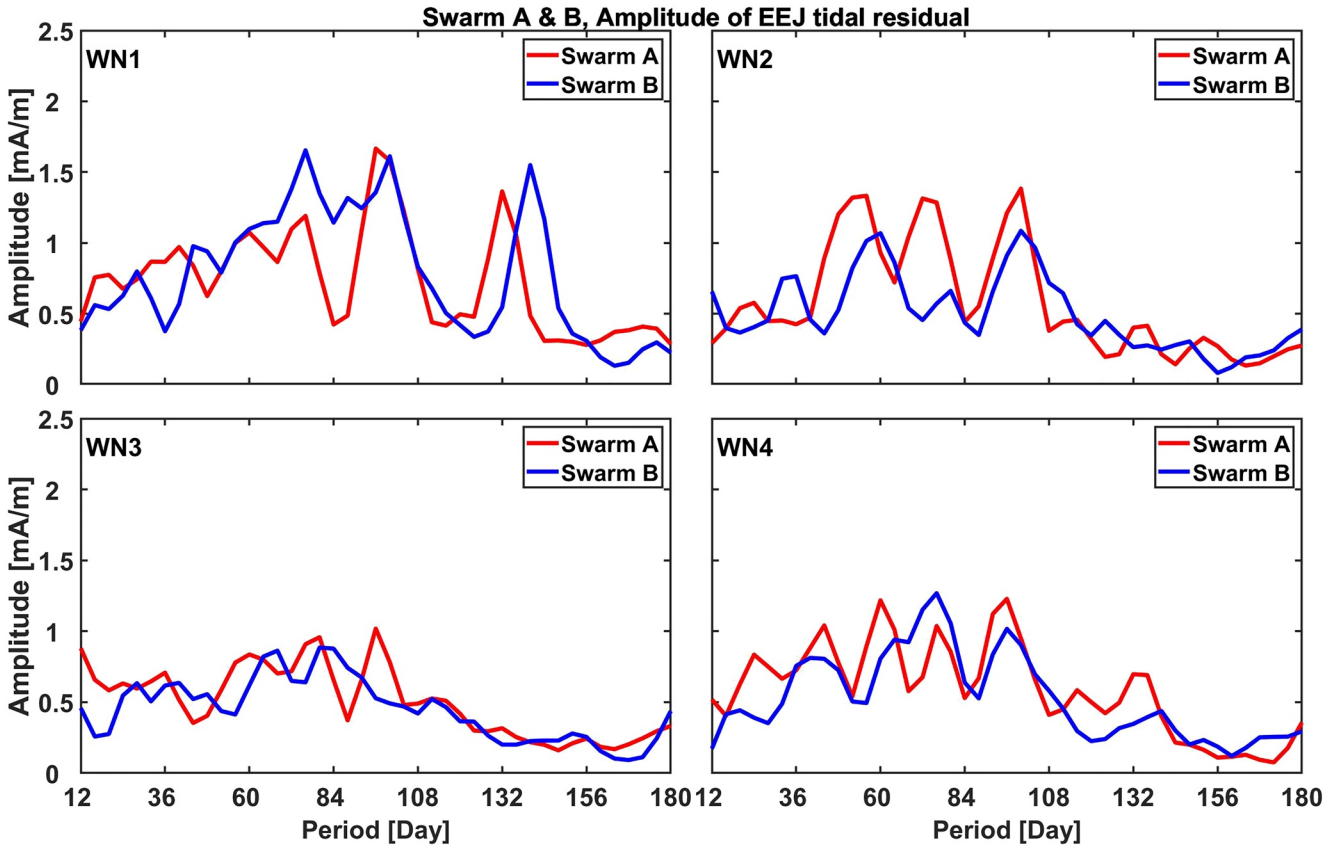

Figure 11. Spectra of the EEJ tidal fluctuations (Figure 10) separately for the four wave numbers and the two satellites. Main peaks in the periodograms can be related to interactions of local time dependences with annual (seasonal) variations and their harmonics.

when tidal activity in EEJ is generally small, is shown in the supporting information (Text, Figure S3). As expected, the local time dependence is less clear there.

For interpreting the results in Figure 13 it is convenient to inspect the ratios along a horizontal line around Swarm B noon-time. This can tell us whether Swarm A detected a stronger or weaker signal at any other local time. Starting with WN-4 (bottom right frame) we find blue color where Swarm B around noontime meets Swarm A from afternoon/evening observations. This means, WN-4 amplitudes get weaker toward evening although they have been corrected for SZA changes. When looking toward Swarm A morning hours we also find negative *ln* values but only slightly smaller than around noon. Obviously, there is a significant weakening of WN-4 signature in EEJ during evening hours.

For WN-3 (lower left frame) a quite different picture emerges. Here warm colors dominate at Swarm A afternoon/evening hours. In particular, for Swarm A around 15 MLT larger ratios are observed than at noontime. During morning hours, the ratios are also slightly above 1 ($ln > 0$). For this wavenumber we find a weakening around noon and an intensification toward the afternoon/evening hours.

A more complex distribution is derived for WN-2 (top right frame). Here the highest negative *ln* values are found during Swarm A afternoon hours (13–15 MLT). While in the morning we obtain positive *ln* values. The WN-2 seems to be well developed in the morning, up to noon, but it decreases significantly toward afternoon hours.

Interestingly, for WN-1 we derive largest amplitudes in the morning hours (enhanced by almost a factor of 2.7, compared to noon). Also in the evening amplitudes are enlarged. This component exhibits smallest amplitudes around noon. Such special behavior suggests that also other processes, not only atmospheric tides, are responsible for the longitudinal patterns at this wavenumber.

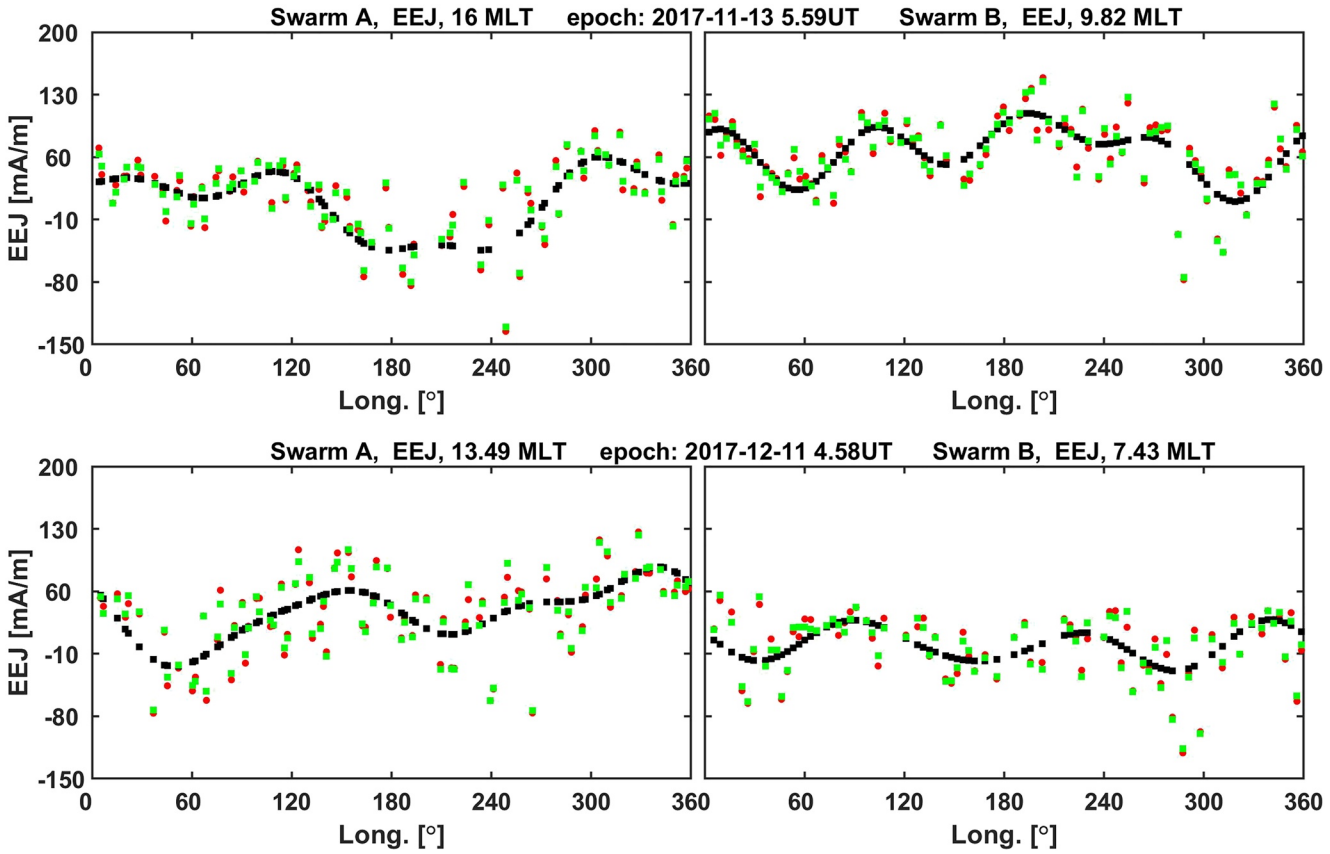

Figure 12. Same format as Figure 2, but for examples with markedly different tidal signatures observed simultaneously by Swarm A and Swarm B.

As mentioned above, during winter and spring seasons the tidal signatures of the EEJ are small. Therefore, the derived local time dependence is expected to be less reliable (see supporting information Text, Figure S3). In any case, quite different patterns of amplitude ratios emerge. They can be interpreted in the same way as described above.

4.4. Variability of the Planetary and Kelvin Wave Activity in the EEJ

In addition to the driving by solar tides we also investigated the modulation of the EEJ by planetary and Kelvin waves. Our dual-point observation data set allows to distinguish between eastward and westward propagating waves. Therefore, we analyzed the planetary-type waves that are covered by our 6-day data sets, e.g., at periods of 1.5, 2, 3, and 6 days occurring at wavenumbers, $s = -1$ and 1. The corresponding function, given in Equation 2, was fitted to the sets of residuals after removal of tidal signatures. The most promising candidates are the westward propagating, $s = 1$, planetary waves with periods of about 6 and 2 days.

The examples presented in Figure 4 demonstrate that these kinds of planetary waves can dominate the activity. For providing a more general overview Figure 14 shows in the top four panels the amplitude variations of the westward propagating planetary waves at various periods over the first 2 years of Swarm data. Related plots for the following 5 years can be found in the supporting information to this paper (Text, Figure S4). Data gaps appear when one of the two spacecraft samples the EEJ at local times near sunrise or sunset (vanishing EEJ signal). The westward 6-day wave is clearly outstanding in this graph (note the larger scale range of that panel). From the derived uncertainty of our wave analysis (Section 4.2) we deduce that waves with amplitudes smaller than 6 mA/m (~2 sigma) should be regarded as insignificant. With this number in mind, amplitudes at other periods stay below that threshold for large parts of the time. Just the westward 6-day wave well sticks out.

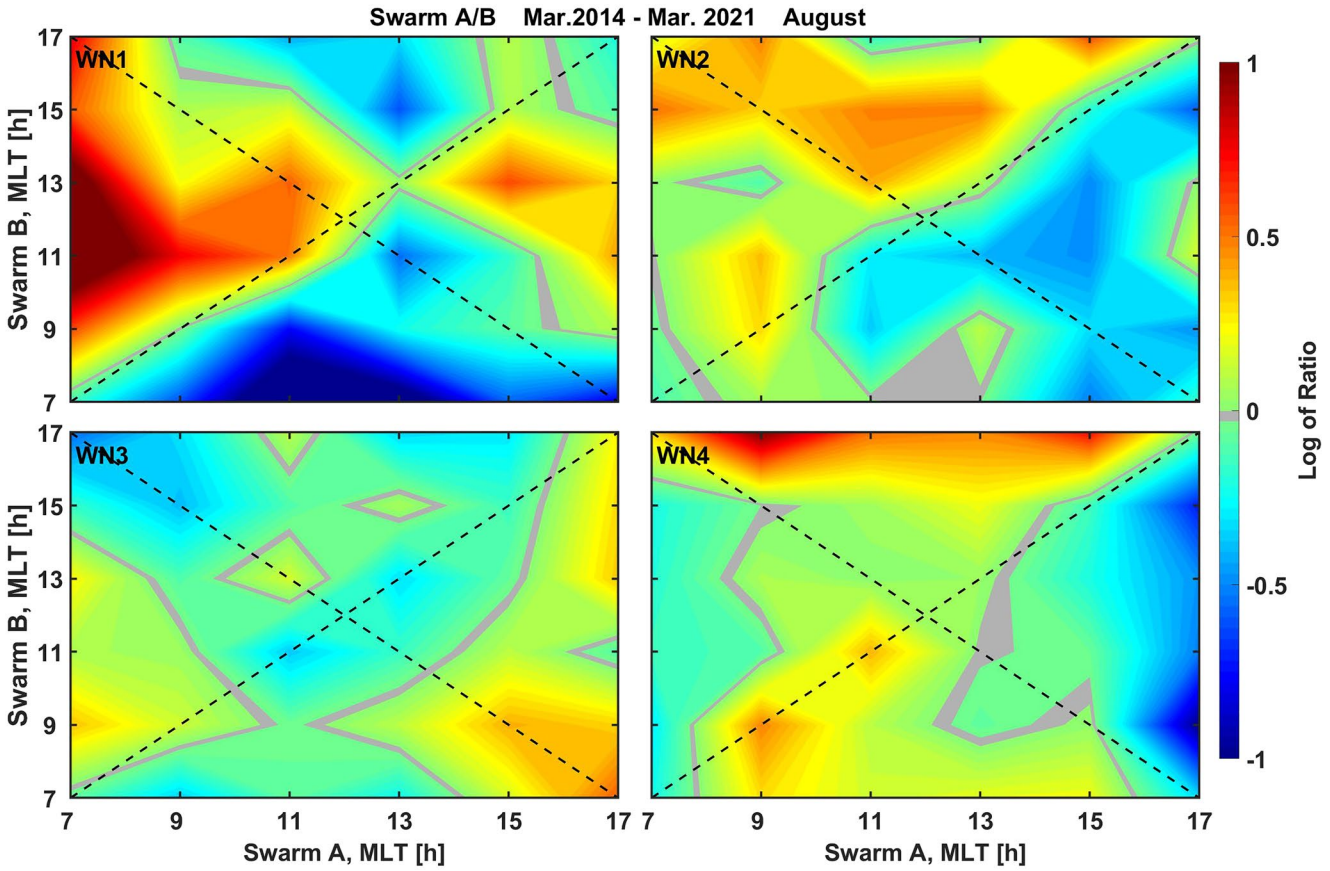

Figure 13. Local-time dependence of EEJ tidal signatures derived simultaneously from Swarm A and Swarm B, separately for the wavenumber 1 through 4 components. Here the mean Log_e values (arithmetic means) of the ratios Swarm A over Swarm B are shown, derived for various local time differences. The data are from the months June to October, when tidal activity is high.

Eastward propagating waves ($s = -1$) with periods of 1.5, 2, 3, 6 days are also shown in Figure 14, lower 4 panels. Largest amplitudes are observed in that set for the 3-day period. We like to relate these wave features to EEJ modulations by ultra-fast Kelvin waves. Forbes, Zhang, et al. (2009) have reported eastward propagating UFKW activity in low latitude mesospheric temperature, which exhibits largest amplitudes around 2–3 days periods at 105 km altitude. Our interpretation of the EEJ modulations at this period is based on the good agreement with UFKW features.

Around September 2014 the westward propagating 6-day wave attains particularly large amplitudes of about 40 mA/m. These are the largest values derived during the 7 years considered here. Generally, the fall equinox seems to be a favorable time for the occurrence of planetary waves near the equator, but also in spring enhanced amplitudes are sometimes observed.

Additional information can be obtained from the phases of the 6-day waves. The phase is defined as the epoch when the wave crest passes the 0° longitude (Greenwich meridian). Since planetary waves are free oscillations of the atmosphere, the absolute value of the phase is of no relevance. But by comparing the phase values of two successive epochs one can deduce the actual period of the quasi-6-day wave and can see whether the derived 6-day wave is part of a continuous wave train or represents an independent oscillation.

Figure 15 shows for the first two years of the Swarm mission, in the lower half, the amplitude of the westward 6-day wave and the phase differences between adjacent events (supporting information, Text, Figure S5, covers the other years). The top frames present the mean solar flux and magnetic activity for each data set. It can be seen that highest solar fluxes, with values up to P10.7 = 180 sfu, occurred during 2014. After that fluxes gradually leveled off during the following years. Conversely, magnetic activity attained its

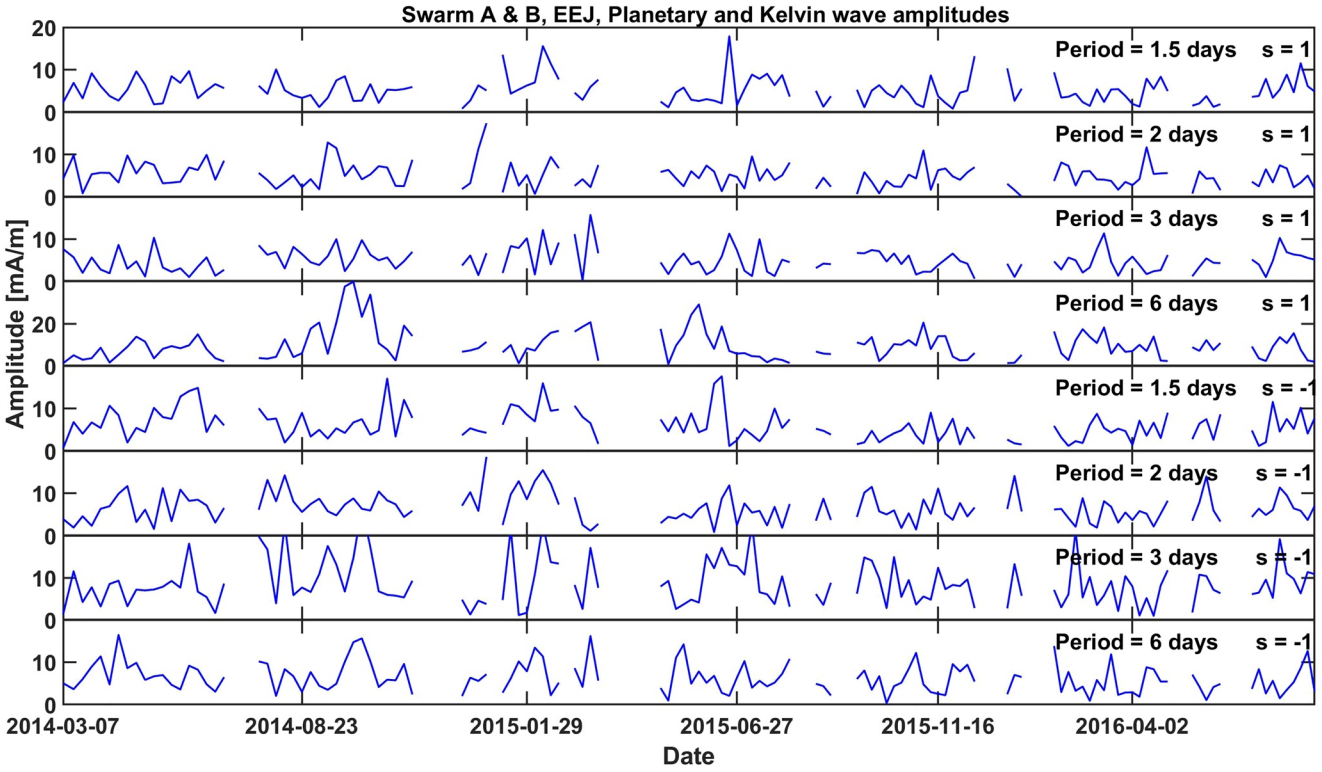

Figure 14. Planetary wave variability of the EEJ, as derived from the combined Swarm A and Swarm B residuals for the two years, March 2014–August 2016. In the top four panels the westward propagating components, $s = 1$, with periods of 1.5, 2, 3, and 6 days are shown. Note the enlarged scale of the 6-day wave. In the four lower panels the eastward propagating ($s = -1$) waves with periods 1.5, 2, 3, and 6 days are presented. The more prominent activity at 3-day periods is related to ultra-fast Kelvin waves.

maximum in 2015 and stayed elevated until the end of 2017. This figure clearly indicates that larger amplitudes of planetary waves in the EEJ occur during times of enhanced solar flux.

Whenever the difference in phase between adjacent epochs is close to 6 days, we can conclude that there is a continuous quasi-6-day oscillation over a longer time. A representative example for that is the fall 2014 season with the large amplitudes, lasting from August 29 to October 16, 2014 where the observed phase differences stay close to 6 days. Here we can determine the mean period of the wave, which amounts to 6.25 days during those weeks. Periods of stable phase differences (continuous 6-day wave trains) are observed repeatedly, mainly accompanied by enhanced amplitudes. For the following examples we derived mean periods, September 2017: 6.3 days, September 2018: 5.8 days, May 2019: 5.6 days. These values are consistent with Forbes and Zhang (2017), who reported an average period of 6.14 days derived from the years 2002–2015. Our gradual decrease of period length could possibly be caused by the decline of the solar activity. This suggestion may be worth to be verified by observations and/or models.

During the later years (see supporting information Text, Figure S5) repeatedly phase differences with values near zero appear. This means, two successive analysis intervals obtain the same epoch for the wave peak at the Greenwich meridian. Since the time spans between spacecraft overtaking reduces to almost 4 days at the end of our analysis (see Figure 1b), which is clearly shorter than the 6-day wave, this is expected.

Peaks in magnetic activity (magnetic storms) obviously disturb the forming of planetary wave signature in EEJ. These active periods (large Ap values) are generally accompanied by a scatter in phase differences. As the solar cycle approaches its minimum, and the magnetic activity decreases, also more stable wave trains are observed.

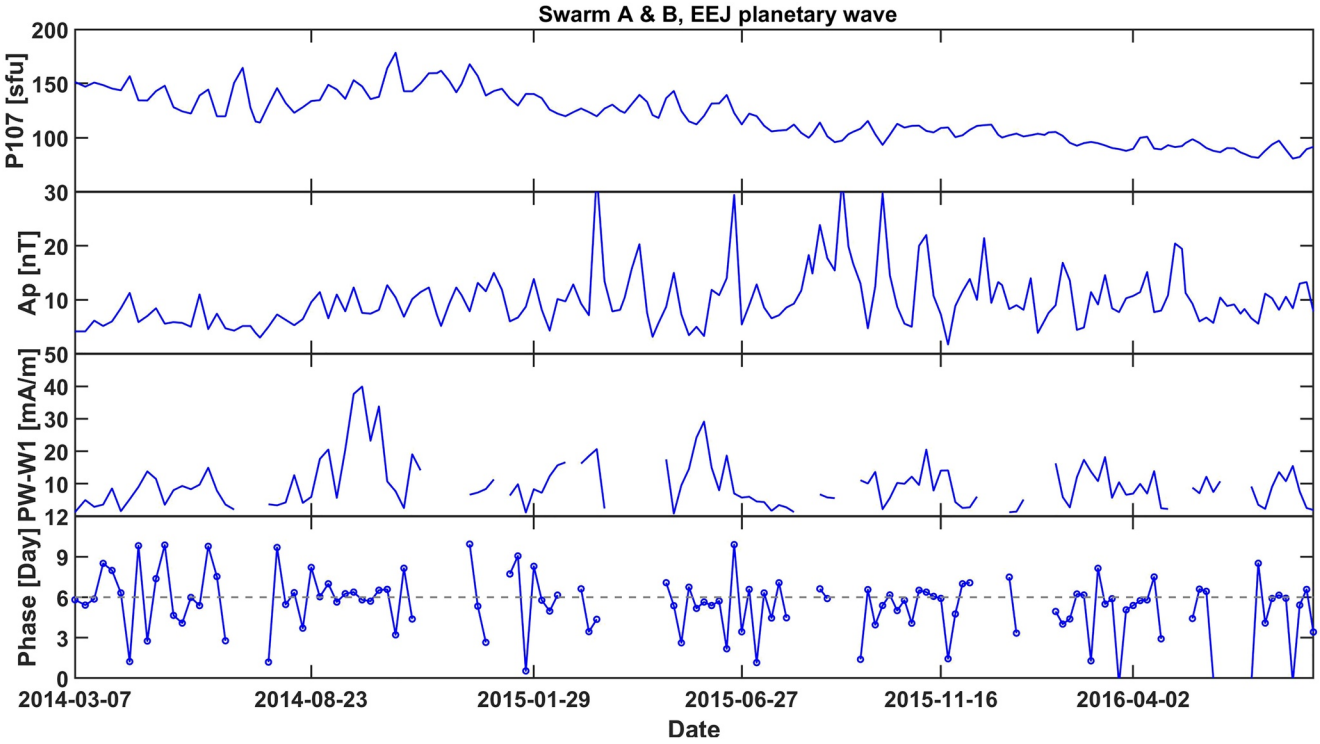

Figure 15. The planetary quasi-6-day wave activity in relation to the solar and magnetic activity. The panels show from top to bottom the 6-day averages of solar flux index, P10.7, daily magnetic activity, Ap, smoothed 6-day wave amplitude and phase difference between adjacent 6-day wave solutions.

5. Discussion

We have presented the modulation of the EEJ by solar tides and by planetary and Kelvin waves. For the first time these wave phenomena are studied from data sampled quasi-simultaneously by spacecraft at two significantly different longitudes. This allows us to derive the variability of all the tidal signatures and other waves from data sets, as short as 6 days. Earlier studies had described in detail the mean characteristics of the EEJ modulation by solar tides (e.g., Lühr & Manoj, 2013 and references therein). But those authors commonly combined observations over several years for finding out average properties. Likewise, Yamazaki et al. (2018) uses data sets of 1 month for studying the influence of planetary waves on the electrojet. Here we have shown that 6 days are enough to determine the effect of tidal and planetary wave activity when data from Swarm A and B are considered simultaneously. This provides an impression of the short-term variability of the EEJ caused by these activities. Due to the high electrical conductivity above the magnetic equator, the EEJ can be regarded as a sensitive indicator of all the electrodynamic processes, which are active in the low-latitude E-layer.

5.1. Causes for Short-Term Tidal Variability

A good impression of the variability caused by tidal effects can be obtained from Figure 6. Amplitudes of the wavenumber components partly more than double up within a week or two and then drop again. Good examples are WN-4 variations. These oscillations can, in particular during late summer to fall season primarily be related to the effect of the eastward propagating diurnal tide, DE3. This tidal component is claimed to be driven by tropical deep convection in the troposphere (Hagan & Forbes, 2002). By interpreting satellite observations of thermospheric density and temperature, as well as electron density variations, supported by atmospheric model runs, Pedatella, Oberheide, et al. (2016) revealed that the short-term (10-day time-scale) variability of the DE3 tidal signal is caused by combined action of three effects: (a) tropospheric forcing, (b) mean winds in the middle atmosphere, and (c) tidal interaction with planetary and gravity waves. They conclude that identifying the source of the short-term tidal variability is complex, and their analysis reveals

that the majority of the variability can be attributed to changes in the troposphere forcing and zonal mean atmosphere conditions.

By applying a harmonic analysis to the EEJ tidal analysis we tried to identify contributions of the various options to the short-term tidal variability. The derived major spectral peaks in Figure 11 can all be related to a beating between local time variation and seasonal variation. The seasonal variation can be related to Item (a) tropospheric forcing and the local time dependent changes to Item (b) the mean state of the middle atmosphere. Higher harmonics of these two drivers cause spectral peaks as short as 30 days. Conversely, we find no clear evidence for the effect of planetary waves (e.g., the prominent quasi-16-day wave) on the EEJ tidal amplitudes. This infers that Item (c) is not so important for the EEJ.

Quite similar arguments may hold for the other wavenumber signals. By comparing the sizes of the corresponding spectral peaks between the wavenumber components, one can estimate the relative importance of the seasonal variation and local time dependence for the EEJ variability.

When looking at the phase data for example, of WN-3 and WN-4 tides (supporting information Text, Figure S2, lower panels) one can see that their values do not change much in relation to the significant short-term amplitude variations. This implies that the tidal system is rather stable. Just the intensity of the driver or the transmission conditions change on time scales of weeks.

In a recent paper Kumari and Oberheide (2020) investigated the dependence of short-term tidal variability on longer-lasting phenomena like the quasi-biannual oscillation (QBO), the El Nino southern oscillation (ENSO), and the solar cycle. They focused in their study on the diurnal nonmigrating tide DE3. Based on SABER mesospheric temperatures they find that the symmetric mode of the DE3 tide dominates during late summer to fall seasons. This low-latitude phenomenon very efficiently modulates the EEJ intensity. Around December solstice DE3 is also active but predominantly as anti-symmetric mode, which affects more the middle latitudes. Their actual latitude, however, depends on the background winds. Occasionally, the mode structure can reach the equator and cause WN-4 patterns in the EEJ, as shown in Figure 12.

We also checked a possible dependence of EEJ tidal signatures on the phase the QBO cycle. For example, Forbes, Zhang, et al. (2008) found a prominent QBO-related interannual variation of the DE3 in the temperature at 100 km altitude. Tidal amplitudes were larger during the westerly phase. This dependence has later been confirmed for DE3 signatures in other quantities like the EEJ or the electron density (e.g., Zhou, Wang, et al., 2016). Conversely, Kumari and Oberheide (2020) report a tendency that the variability of the DE3 symmetric mode, which is mainly responsible for related signatures in the EEJ, is enhanced during the easterly QBO phase. For checking that result we inspected our EEJ tidal variability. Basis for that are the tidal amplitude variations presented in Figure 10. For characterizing their main amplitudes, we calculated RMS values over 140 days (local time cycle). Then the interval is shifted by 70 days and the RMS calculation repeated. Obtained results of RMS variation over the years are shown in Figure 16. Overall, the RMS variation is rather small, staying within the range of ±2 mA/m for all wave numbers. Most prominent features are the seasonal variations, exhibiting peaks at similar dates every year. WN-1 makes an exception.

In the bottom panel of Figure 16 the low-latitude stratospheric zonal wind velocity at 20 hPa is plotted. Its changing direction represents the QBO. Positive values stand for westerly winds. From the comparison with the RMS curves no clear correlation with the QBO phase can be deduced for any of the wave numbers. According to Kumari and Oberheide (2020) the DE3 fluctuations are larger for negative winds. This should result in larger RMS values of the WN-4 EEJ fluctuations. When considering the peaks in WN-4 at the beginning of 2015, fall 2017, and end of 2019 some tendency of enhanced fluctuation level for easterlies may be stated. However, for making firm statements on the influence of the QBO phase on the fluctuation level of tidal signature in the EEJ longer data sets are required.

5.2. Local Time Dependence of Tidal Signatures

The Swarm constellation of satellites enables us for the first time to study tidal signatures of the EEJ simultaneously at two local times on global scale. Over the years Swarm A and Swarm B covered the whole range of local time differences. By definition, tides are global-scale oscillations, and their amplitudes are independent of local time. However, the interaction of two or more tidal components can cause wavenumber

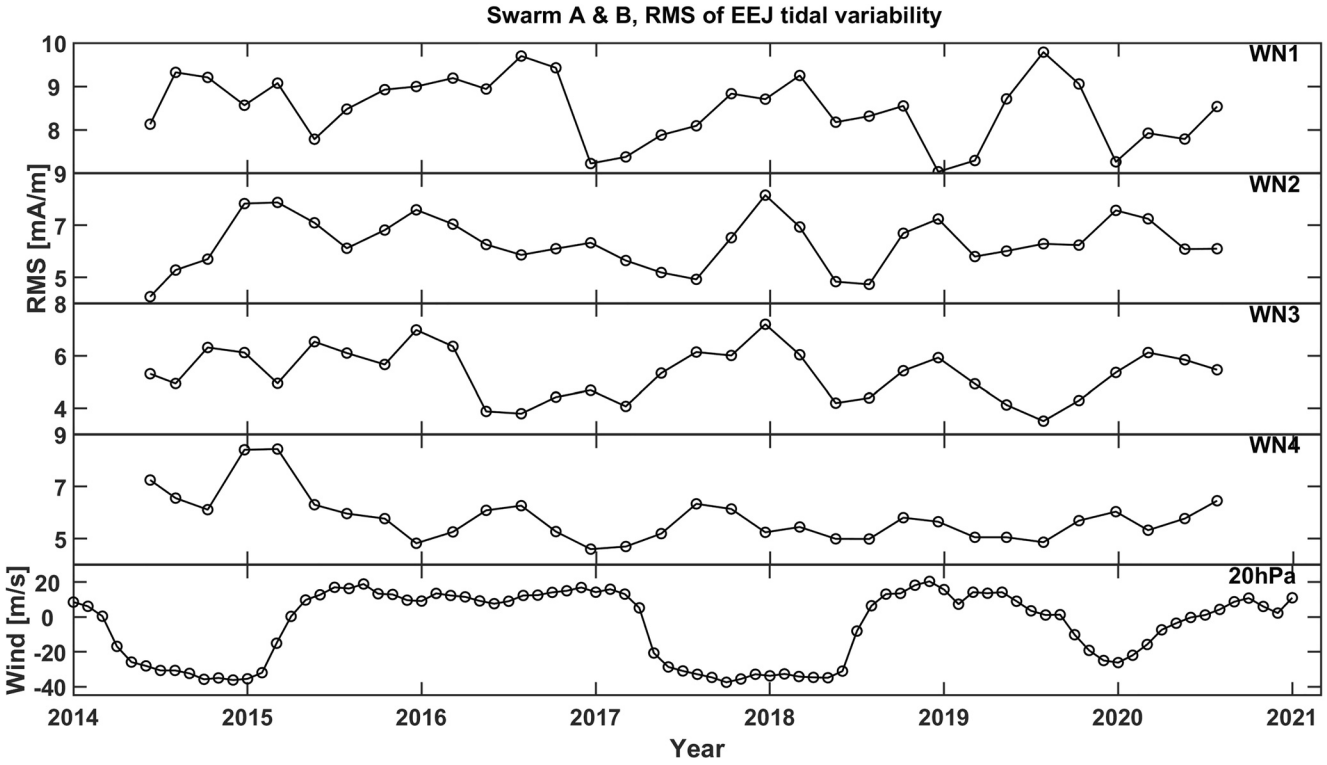

Figure 16. RMS values of the EEJ tidal fluctuations shown in Figure 10. Shown are averages over a whole local time cycle (140 days). Low-latitude stratospheric zonal winds in the bottom panel reflect the QBO cycle. Positive values represent the westerly phase of QBO.

patterns with varying amplitude over local time. The two Swarm satellites generally return quite different wavenumber spectra when sampling the EEJ at the same epoch but at different local times (e.g., Figure 12). These differences between local times do not seem to occur randomly, but show systematic patterns. Mean amplitudes ratios of EEJ tidal signatures between morning or evening and noon-time are displayed in Figure 13, separately for all wave numbers. One possibility could be that the tidal propagation conditions from the lower atmosphere to the ionosphere change over the course of a day. According to Pedatella, Oberheide, et al. (2016) propagation conditions depend on the vertical wavelength and the zonal mean background winds.

However, when looking at WN-3 and WN-4 variations in Figure 13 we find enhancements and reduction in the evening, respectively. These two wavenumbers are primarily caused by DE2 and DE3 tides. Both are propagating up from troposphere. Therefore, they are expected to be influences in a similar way by the background wind. It thus is not well suited for explaining the contrasting local time variations. A better argument for WN-4 is the partial contribution of DW5, besides DE3, to this wavenumber. When both tidal components have phase values close to 12 LT, the wavenumber peaks at noon-time and fall off toward morning and evening. Just these properties of the two tidal components have been reported by Lühr and Manoj (2013) (their Table 3). Similarly, for WN-3, here Lühr and Manoj (2013) list as main contributors the components DE2, SE1, and SPW3 during late summer and fall season. When combining these three with their observed phases the weakened noon-time amplitude appears, compared to morning and evening results.

For wavenumber 1 we find a significant increase of amplitude toward morning hours. It also increases toward the evening but not as much. This longitudinal pattern in EEJ amplitude shows particular characteristics in a number of features. Their origin is probably not dominated by tidal driving. There are a number of other facts that contribute to a wave-1 longitudinal pattern of the EEJ. Among them are the geomagnetic field intensity at the magnetic equator, the ocean/continent distribution and the latitudinal displacement

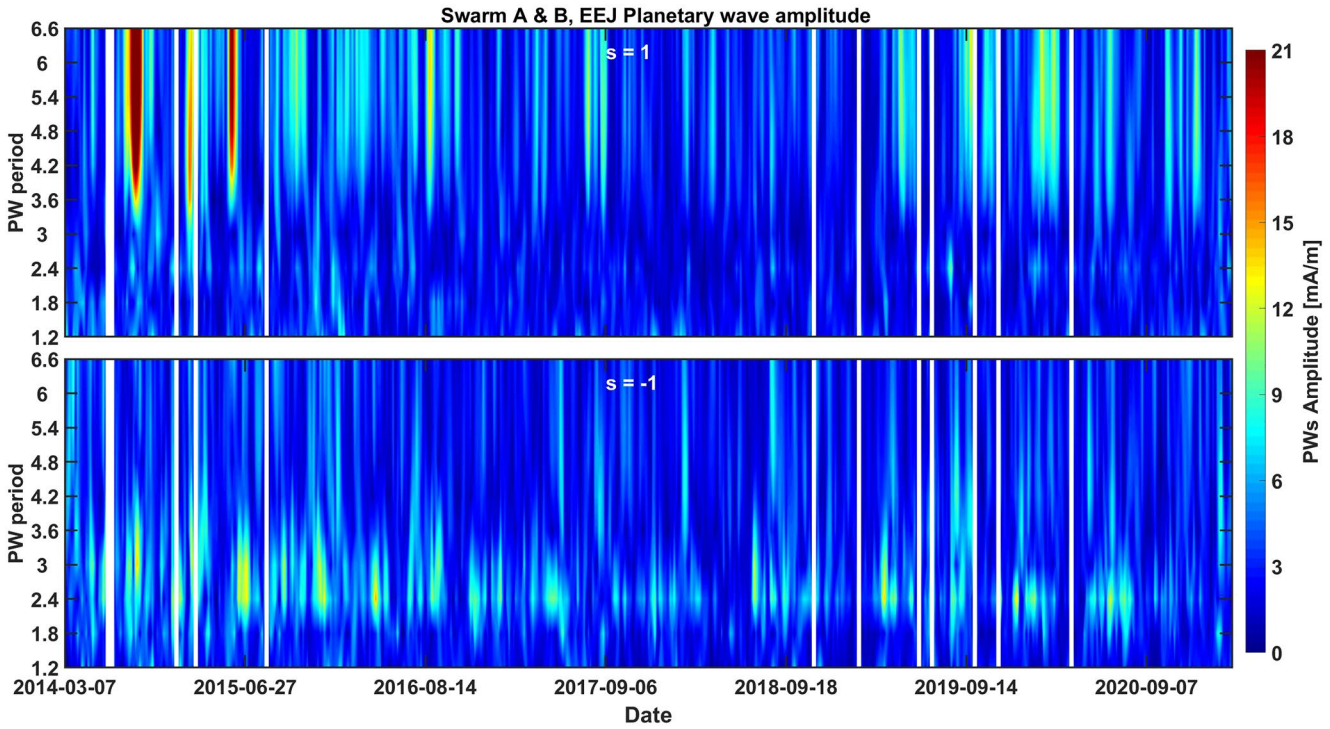

Figure 17. Dynamic spectra of EEJ modulation by planetary-type waves in the period range up to 6 days. The top frame shows westward propagating planetary waves with wavenumber 1 ($s = 1$), and at the bottom eastward propagating ($s = -1$) waves are presented. Enhanced signatures in the lower frame around 2.4 days are associated with ultralow Kelvin waves. Note, wave amplitudes have not been normalized.

of the magnetic equator. Other kinds of analyses than applied here, would be needed for isolating the tidal effects within WN-1.

5.3. Features of the Planetary and Kelvin Waves

The Swarm observations of the EEJ at two well separated longitudes enable us to monitor both influences from tidal and planetary wave activity. Opposed to single-satellite observations, we can distinguish eastward from westward propagating planetary waves with the multi-point Swarm measurements. Figure 17 shows dynamic spectra of westward and eastward propagating waves. The westward propagating signatures, in the top frame, are associated with planetary waves. Within the covered spectral range, the quasi-6-day wave is most prominently modulating the EEJ, as has earlier been stated (e.g., Yamazaki et al., 2018). Its effect is, as expected, spread over quite a range of periods. The quasi-2-day planetary wave appears also from time to time, but at significantly lower amplitude. We observe a clear control of the planetary wave amplitudes by the solar flux level. This can partly be explained by the enhanced ionospheric conductivity that causes more intense EEJs. During the first year, with flux values varying around P10.7 = 150 sfu, the largest 6-day waves are found (see Figure 14). During the solar minimum with flux values around P10.7 = 70 the 6-day wave amplitude falls partly below 10 mA/m. It would be worth studying the dependence of planetary wave signatures in the stratosphere-mesosphere on solar flux level because they are considered as source regions for the EEJ modulation.

It is indicated by Yamazaki et al. (2018) that the quasi-6-day wave signature in the EEJ is stronger at some longitudes than at others. With our dual-point wave analysis, assuming constant wave amplitudes at all longitudes, such apparent amplitude differences are interpreted as interferences between planetary waves with different periods, reflected by the spectrum.

Obviously, there seems to be a seasonal dependence of planetary wave activity. For example, Forbes and Zhang (2017), studying the quasi-6-day planetary waves signature in mesospheric temperature, find largest amplitudes at mid latitudes around 40° Lat. Preferred seasons for large waves are April and late summer.

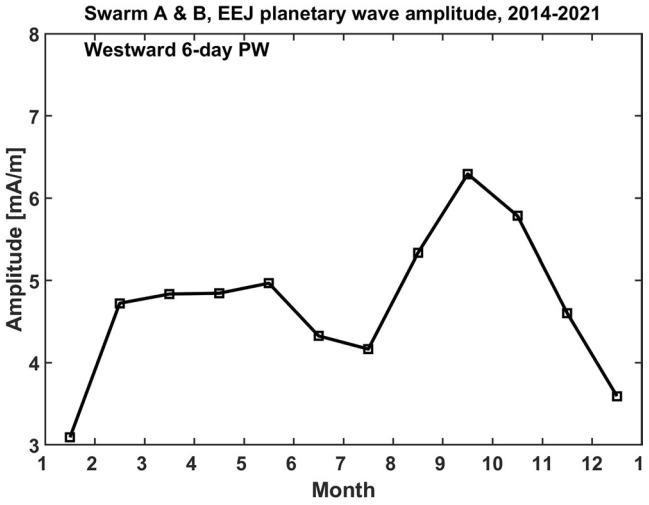

Figure 18. Mean seasonal variation of the EEJ modulation by the quasi-6-day planetary wave.

The equatorial region is almost void of quasi-6-day signal. Appreciable wave amplitudes near the equator are found in the mesosphere during months around August. This is quite consistent with our observations of largest amplitudes and fairly stable 6-day wave oscillations in late summer and fall seasons. For determining the mean seasonal variability of the EEJ modulation by quasi-6-day waves we sorted all the amplitudes derived over the years (see Figure 14) into month of year bins. The resulting annual variation is shown in Figure 18. Our 6-day wave exhibits a clear peak for September and a rather flat plateau around spring time. This is in good agreement with the equatorial activity of the quasi-6-day wave in mesospheric temperature, as shown by Forbes and Zhang (2017) (see their Figure 3). It further supports the inferred connection between mesospheric planetary waves and associated EEJ modulations.

Overall, we can state, the planetary waves play, compared to the solar tidal influence, only a minor role in modulating the electrojet amplitude. During months of enhanced amplitudes (around September) the 6-day planetary wave effect on EEJ ranges only around 30% of that caused by the tides (compare Figures 7 and 18). During other months the effect of planetary waves reduces even further, to about half of that value.

Some authors claim the generation of child waves, caused by the interaction between the 6-day wave and diurnal and semi-diurnal migrating tides (e.g., Gan, Oberheide et al., 2017). However, due to the minor importance of this planetary wave component at the equator, we do not expect significant contributions to the tidal variability in the EEJ. Furthermore, with the limited spectral resolution of our analysis, it is also not possible to identify such child waves from our data set.

A new item is the modulation of EEJ intensity by ultra-fast Kelvin waves. These effects have never been reported before. In Figure 17, lower frame, wave features around 2.4 days are clearly sticking out. We interpret these eastward propagating ($s = -1$) oscillations as UFKW. According to Forbes, Zhang, et al. (2009) UFKW are low-latitude phenomena and occur sporadically at any time of the year. The good agreement between our 2.4-day signatures in the EEJ and the related features of the thermospheric temperature reported by Forbes, Zhang, et al. (2009), peaking at periods of 2–3 days around 105 km, support our inference that these EEJ wave signatures are driven by UFKW.

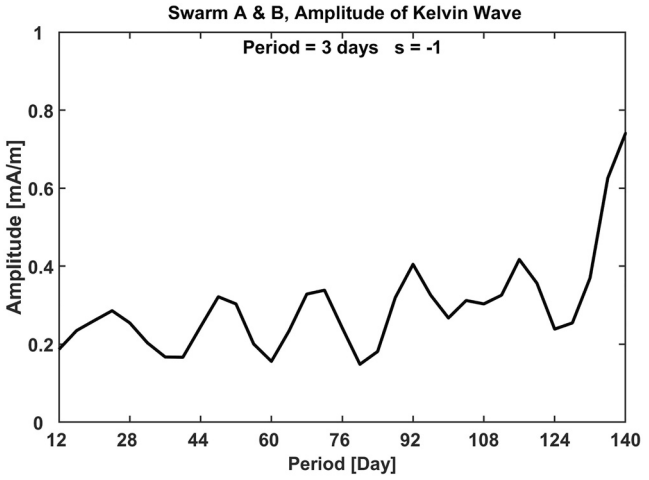

Figure 19. Periodogram of the 3-day ultra-fast Kelvin wave activity in the EEJ derived from the years 2014–2021. Within a 140-day interval all local times are covered. Amplitudes have not been normalized.

Forbes, Zhang, et al. (2009) looked among others into the periodicities, at which UFKW activity appears. We also determined the mean spectrum of the 3-day ($s = -1$) amplitude variability (see Figure 14) over all the years considered. The resulting periodogram is presented in Figure 19. Clear spectral peaks are found at periods of 24, 48, 68, 92, 116, and 140 days. The rather regular series of peaks appears at separations of about 24-day periods. A corresponding periodogram presented by Forbes, Zhang, et al. (2009) (their Figure 7) exhibits peaks at 31, 40, and 55 days. Here are the separations about half as large. These authors considered sliding periods of only 60 days (the time needed for TIMED to cover all local times) for their spectral analysis. Therefore, they obtained higher resolution but a shorter period range. Swarm satellites require about 140 days for the local time cycle. Therefore, a larger range of periods can be covered, at the expense of lower resolution. Although totally different years are considered, the resulting spectra show some similarity at shorter periods. Our 24-day peak may be related to their 31-day result, and our 48-day with their 55-day peak.

Forbes, Zhang, et al. (2009) suggest some connection of the UFKW activity with the intensity of the diurnal migrating tide and/or the intra-seasonal

oscillation of the zonal mean atmosphere. For the shorter period peaks, they find a good agreement with the activity variation of the diurnal tide. Our longer-period UFKW spectral peaks are most probably controlled by the intra-seasonal oscillations. Indications in that direction are provided by Forbes, Zhang, et al. (2009) in their Figure 7, top frame. But for a solid explanation of the UFKW variability at E-layer height more research is needed.

6. Summary and Conclusions

In this study we have investigated the modulation of the EEJ by solar tides and planetary waves. Special emphasis is put on the short-term variability of these wave phenomena. The analysis is based on two-point measurements from the Swarm A and Swarm B spacecraft. Individual, 6-day long data sets are used for evaluating both the solar tidal and the planetary wave signals in the EEJ. From these fairly short analysis intervals, the week-to-week changes of the EEJ modulation have been deduced for the first time. Main findings of our investigations can be summarized as follows:

1. When averaging the individual 6-day results of tidal signatures over the 7 years of Swarm data considered here the well-known seasonal variations of the different wavenumber components emerge. This provides confidence in the analysis of our short-period data sets which are the basis for further investigations.
2. The EEJ tidal signatures vary significantly from week to week. Conversely, the phases of these signals vary only smoothly. This suggests that either the intensity of the driving processes in the lower atmosphere vary on these time scales or the propagation conditions through the middle atmosphere to the ionosphere change. While the atmospheric tidal system in the source region is obviously not changing on short-terms.
3. Spectral analysis of the tidal variability reveals that the beating of local time dependence with annual amplitude variations (and harmonics of both periods) are the main contributors to the EEJ short-term fluctuation. This suggests that the intra-annual variability of the source combined with the changing interactions of the different tidal components, causing local time dependences, are mainly responsible for the variability.
4. The various wavenumber components exhibit different dependences on local time. The well-known tide DE3, main contributor to WN-4, shows a clear amplitude depression around evening hours, with respect to noontime. This is explained by an additional contribution from DW5. Different from that WN-3, mainly controlled by DE2, becomes stronger in the afternoon and in the morning. Possible reason for those local time dependences are additional contributions by SPW3 and SE1 tidal components. Particularly outstanding are the enhanced amplitudes of wavenumber-1 oscillations in the morning and somewhat less also in the evening. These large signals are probably caused predominantly by longitude dependent characteristics of the EEJ, not by tides.
5. By combining the data from Swarm A and B we were able to determine also the planetary wave activity in the EEJ. In our 6-day data sets the westward propagating quasi-6-day wave is clearly the dominating. Next in line is the 2-day wave. The quasi-6-day wave shows a clear seasonal variation with an occurrence peak around September and lesser rates during spring. Overall, this planetary wave is fairly weak at low latitudes, contributing hardly 30% to the modulation of the EEJ compared to that coming from solar tides.
6. From our dual-satellite data set also eastward propagating waves can be determined. We interpret the enhanced activity in the 2–3 days period range as caused by ultra-fast Kelvin waves. The effects of these waves on the EEJ are studied for the first time here. UFKW activity appears sporadically with repeating intervals of 1–4 months. The effect on the EEJ is even smaller than that of the quasi-6-day planetary wave.

This initial study of the short-term variability of the EEJ modulation has revealed a number of new results. But at the same time several questions remain. What are the actual processes causing the prominent local time dependence of WN-1 signatures in the EEJ? Or what is the role of gravity waves in controlling the short-term variations. Addressing all these open issues requires interdisciplinary approaches and/or modeling efforts to provide answers.

Data Availability Statement

The data used here are the Swarm Level-2 CAT2 "Equatorial Electrojet," which are freely available at https://earth.esa.int/web/guest/swarm/data-access.

Acknowledgments
The authors thank the European Space Agency for providing the Swarm data and for supporting the development of Swarm Level-2 processing algorithms. The work of Yun-Liang Zhou is supported by the National Key R&D Program of China (No. 2018YFC1407303).

References

Alken, P. (2020). Estimating currents and electric fields at low latitudes from satellite magnetic measurements. In M. W. Dunlop & H. Lühr (Eds.), Ionospheric multi-spacecraft analysis tools. ISSI Scientific Report Series (Vol. 17, pp. 117–140). Springer Nature.

Alken, P., & Maus, S. (2010). Electric fields in the equatorial ionosphere derived from CHAMP satellite magnetic field measurements. *Journal of Atmospheric and Solar-Terrestrial Physics*, *72*(4), 319–326. https://doi.org/10.1016/j.jastp.2009.02.006

Alken, P., Maus, S., Chulliat, A., & Manoj, C. (2015a). NOAA/NGDC candidate models for the 12th generation International Geomagnetic Reference Field. *Earth, Planets and Space*, *67*, 68. https://doi.org/10.1186/s40623-015-0215-1

Alken, P., Maus, S., Chulliat, A., Vigneron, P., Sirol, O., & Hulot, G. (2015b). Swarm equatorial electric field chain: First results. *Geophysical Research Letters*, *42*(3), 673–680. https://doi.org/10.1002/2014GL062658

England, S. L. (2012). A review of the effects of non-migrating atmospheric tides on the Earth's low-latitude ionosphere. *Space Science Reviews*, *168*(1), 211–236. https://doi.org/10.1007/s11214-011-9842-4

England, S. L., Liu, G., Zhou, Q., Immel, T. J., Kumar, K. K., & Ramkumar, G. (2012). On the signature of the quasi-3-day wave in the thermosphere during the January 2010 URSI World Day Campaign. *Journal of Geophysical Research*, *117*(A6). https://doi.org/10.1029/2012JA017558

England, S. L., Maus, S., Immel, T. J., & Mende, S. B. (2006). Longitudinal variation of the E-region electric fields caused by atmospheric tides. *Geophysical Research Letters*, *33*(21), L21105. https://doi.org/10.1029/2006GL027465

Forbes, J. M. (1981). The equatorial electrojet. *Reviews of Geophysics*, *19*(3), 469–504. https://doi.org/10.1029/RG019i003p00469

Forbes, J. M. (1995). Tidal and planetary waves. In R. M. Johnson & T. L. Killeen (Eds.), The upper mesosphere and lower thermosphere: A review of experiment and theory, geophysical monograph (Vol. 87). AGU.

Forbes, J. M. (2000). Wave coupling between the lower and upper atmosphere: Case study of an ultra-fast Kelvin wave. *Journal of Atmospheric and Solar-Terrestrial Physics*, *62*(17–18), 1603–1621. https://doi.org/10.1016/S1364-6826(00)00115-2

Forbes, J. M., Hagan, M. E., Miyahara, S., Miyoshi, Y., & Zhang, X. (2003). Diurnal nonmigrating tides in the tropical lower thermosphere. *Earth, Planets and Space*, *55*(7), 419–426. https://doi.org/10.1186/bf03351775

Forbes, J. M., & Zhang, X. (2017). The quasi-6 day wave and its interactions with solar tides. *Journal of Geophysical Research: Space Physics*, *122*(4), 4764–4776. https://doi.org/10.1002/2017JA023954

Forbes, J. M., Zhang, X., Palo, S., Russell, J., Mertens, C. J., & Mlynczak, M. (2008). Tidal variability in the ionospheric dynamo region. *Journal of Geophysical Research*, *113*(A2). https://doi.org/10.1029/2007JA012737

Forbes, J. M., Zhang, X., Palo, S. E., Russell, J., Mertens, C. J., & Mlynczak, M. (2009). Kelvin waves in stratosphere, mesosphere and lower thermosphere temperatures as observed by TIMED/SABER during 2002–2006. *Earth, Planets and Space*, *61*(4), 447–453. https://doi.org/10.1186/bf03353161

Friis-Christensen, E., Lühr, H., Knudsen, D., & Haagmans, R. (2008). Swarm – An Earth Observation Mission investigating Geospace. *Advances in Space Research*, *41*(1), 210–216. https://doi.org/10.1016/j.asr.2006.10.008

Gan, Q., Oberheide, J., Yue, J., & Wang, W. (2017). Short-term variability in the ionosphere due to the nonlinear interaction between the 6-day wave and migrating tides. *Journal of Geophysical Research: Space Physics*, *122*(8), 8831–8846. https://doi.org/10.1002/2017JA023947

Gu, S.-Y., Dou, X., Lei, J., Li, T., Luan, X., Wan, W., & Russell, J. M., III (2014). Ionospheric response to the ultrafast Kelvin wave in the MLT region. *Journal of Geophysical Research: Space Physics*, *119*(2), 1369–1380. https://doi.org/10.1002/2013JA019086

Hagan, M. E., & Forbes, J. M. (2002). Migrating and nonmigrating diurnal tides in the middle and upper atmosphere excited by tropospheric latent heat release. *Journal of Geophysical Research*, *107*(D24), 4754. https://doi.org/10.1029/2001JD001236

Hagan, M. E., & Roble, R. G. (2001). Modeling diurnal tidal variability with the National Center for Atmospheric Research thermosphere-ionosphere-mesosphere-electrodynamics general circulation model. *Journal of Geophysical Research*, *106*(A11), 24869–24882. https://doi.org/10.1029/2001ja000057

Immel, T. J., Sagawa, E., England, S. L., Henderson, S. B., Hagan, M. E., Mende, S. B., et al. (2006). Control of equatorial ionospheric morphology by atmospheric tides. *Geophysical Research Letters*, *33*(15), L15108. https://doi.org/10.1029/2006GL026161

Kumari, K., & Oberheide, J. (2020). QBO, ENSO, and solar cycle effects in short-term nonmigrating tidal variability on planetary wave timescales from SABER—An information-theoretic approach. *Journal of Geophysical Research: Atmospheres*, *125*(6), e2019JD031910. https://doi.org/10.1029/2019JD031910

Lühr, H., & Manoj, C. (2013). The complete spectrum of the equatorial electrojet related to solar tides: CHAMP observations. *Annales Geophysicae*, *31*(8), 1315–1331. https://doi.org/10.5194/angeo-31-1315-2013

Lühr, H., & Maus, S. (2010). Solar cycle dependence of quiet-time magnetospheric currents and a model of their near-Earth magnetic fields. *Earth, Planets and Space*, *62*(10), 843–848. https://doi.org/10.5047/eps.2010.07.012

Lühr, H., Rother, M., Häusler, K., Alken, P., & Maus, S. (2008). The influence of nonmigrating tides on the longitudinal variation of the equatorial electrojet. *Journal of Geophysical Research*, *113*(A8). https://doi.org/10.1029/2008JA013064

Lühr, H., Rother, M., Häusler, K., Fejer, B., & Alken, P. (2012). Direct comparison of nonmigrating tidal signatures in the electrojet, vertical plasma drift and equatorial ionization anomaly. *Journal of Atmospheric and Solar-Terrestrial Physics*, *75–76*, 31–43. https://doi.org/10.1016/j.jastp.2011.07.009

Manoj, C., Maus, S., Lühr, H., & Alken, P. (2008). Penetration characteristics of the interplanetary electric field to the daytime equatorial ionosphere. *Journal of Geophysical Research*, *113*(A12). https://doi.org/10.1029/2008JA013381

Maus, S., Yin, F., Lühr, H., Manoj, C., Rother, M., Rauberg, J., et al. (2008). Resolution of direction of oceanic magnetic lineations by the sixth-generation lithospheric magnetic field model from CHAMP satellite magnetic measurements. *Geochemistry, Geophysics, Geosystems*, *9*(7), Q07021. https://doi.org/10.1029/2008GC001949

Oberheide, J., Wu, Q., Killeen, T. L., Hagan, M. E., & Roble, R. G. (2006). Diurnal nonmigrating tides from TIMED Doppler Interferometer wind data: Monthly climatologies and seasonal variations. *Journal of Geophysical Research*, *111*(10), A10S03. https://doi.org/10.1029/2005JA011491

Pedatella, N. M., Forbes, J. M., & Oberheide, J. (2008). Intra-annual variability of the low-latitude ionosphere due to nonmigrating tides. *Geophysical Research Letters*, *35*(18), L18104. https://doi.org/10.1029/2008GL035332

Pedatella, N. M., Oberheide, J., Sutton, E. K., Liu, H. L., Anderson, J. L., & Raeder, K. (2016). Short-term nonmigrating tide variability in the mesosphere, thermosphere, and ionosphere. *Journal of Geophysical Research: Space Physics*, *121*(4), 3621–3633. https://doi.org/10.1002/2016JA022528

Sagawa, E., Immel, T. J., Frey, H. U., & Mende, S. B. (2005). Longitudinal structure of the equatorial anomaly in the nighttime ionosphere observed by IMAGE/FUV. *Journal of Geophysical Research*, *110*(A11), A11302. https://doi.org/10.1029/2004JA010848

Salby, M. L. (1984). Survey of planetary-scale traveling waves: The state of theory and observations. *Reviews of Geophysics*, *22*(2), 209–236. https://doi.org/10.1029/rg022i002p00209

Salby, M. L., & Garcia, R. R. (1987). Transient response to localized episodic heating in the tropics. Part I: Excitation and short-time near-field behavior. *Journal of the Atmospheric Sciences*, *44*(2), 458–498. https://doi.org/10.1175/1520-0469(1987)044<0458:TRTLEH>2.0.CO;2

Salby, M. L., Hartmann, D. L., Bailey, P. L., & Gille, J. C. (1984). Evidence for equatorial Kelvin modes in Nimbus-7 LIMS. *Journal of the Atmospheric Sciences*, *41*(2), 220–235. https://doi.org/10.1175/1520-0469(1984)041<0220:EFEKMI>2.0.CO;2

Yamazaki, Y., Stolle, C., Matzka, J., & Alken, P. (2018). Quasi-6-day wave modulation of the equatorial electrojet. *Journal of Geophysical Research: Space Physics*, *123*(5), 4094–4109. https://doi.org/10.1029/2018JA025365

Zhou, Y.-L., Lühr, H., Alken, P., & Xiong, C. (2016a). New perspectives on equatorial electrojet tidal characteristics derived from the Swarm constellation. *Journal of Geophysical Research: Space Physics*, *121*(7), 7226–7237. https://doi.org/10.1002/2016JA022713

Zhou, Y.-L., Lühr, H., Xu, H.-W., & Alken, P. (2018). Comprehensive analysis of the counter equatorial electrojet: Average properties as deduced from CHAMP observations. *Journal of Geophysical Research: Space Physics*, *123*(6), 5159–5181. https://doi.org/10.1029/2018JA02552610.1029/2018ja025526

Zhou, Y.-L., Wang, L., Xiong, C., Lühr, H., & Ma, S.-Y. (2016b). The solar activity dependence of nonmigrating tides in electron density at low and middle latitudes observed by CHAMP and GRACE. *Annales Geophysicae*, *34*(4), 463–472. https://doi.org/10.5194/angeo-34-463-2016